Physics – Uspekhi **44** (8) 761 – 783 (2001)

REVIEWS OF TOPICAL PROBLEMS PACS numbers: 68.35.Rh, **68.65.+g**, 71.10.Pm, **73.61.–r**

β-SiC(100) surface: atomic structures and electronic properties

V Yu Aristov

DOI: 10.1070/PU2001v044n08ABEH000979

Contents

Abstract. This review organizes and presents the state of the art of research related to the composition, atomic and electronic structure, and electronic properties of various superstructures that were recently shown to exist on clean β-SiC(100) surfaces. In the past 10 years, considerable experimental and theoretical progress in clean β-SiC(100) surfaces has been made. In particular, various surface reconstructions have been identified and studied, and the controlled formation of highly stable, very long straight lines of Si dimers self-organizing on a β-SiC(100) surface have been found, with the line separation being determined by the annealing time and temperature. Many aspects of the field (composition, unit cell models, etc.) are still subject to debate, however.

1. Introduction

Largely because of the birth and rapid development of microelectronics, we have become spectators of, and some of us participants in, a huge number of studies in the field of 'commonplace' semiconductors. These studies have led to fantastic progress in various fields of technology and, especially, in developing and building computers. Only 7–10 years ago it would be impossible to imagine a pocket-sized computer with a 250-MB RAM. Even the capacity of the hard disk of a standard IBM-compatible computer was usually 40 MB. However, in the last decade or so researchers have begun to focus on what is known as 'unconventional' materials, and among these the most important materials were compounds of elements of group IV, or IV–IV compounds. This is not accidental, since judging from the number of publications in, at least, solid state physics, the unquestionable leader in the last twenty to thirty years have been group-IV elements.

The present review is devoted to silicon carbide, SiC, which is the only binary compound of the elements belonging to group IV that exists in the solid phase. More exactly, we will be dealing with the surface (100) of the cubic phase of SiC (β-SiC). Silicon carbide has been used as a material for a fairly long time. In the mid-1980s several papers were published that dealt with the surface of silicon carbide, but actually intensive studies of the surface of this semiconductor began less than 10 years ago, after a method had been developed for preparing the surface in a more or less reproducible way. The situation was quite similar to that in semiconductor physics, i.e., although the first studies were conducted in the 1930s, a clear understanding of the phenomena and the tremendous upgrowth began only in the 1950s, when a way of fabricating extremely pure semiconductor crystals and then doping them in a controlled manner was developed.

As it turned out, the β-SiC(100) surface and the material itself too, exhibit amazing properties, which sets them apart from, say, silicon. These properties could even now be used to

V Yu Aristov Institute of Solid State Physics,
Russian Academy of Sciences,
142432, Chernogolovka, Moscow Region, Russian Federation
Tel. (7-095) 993-27 55. Fax (7-096) 524-97 01
E-mail: aristov@issp.ac.ru

Received 29 March 2001
Uspekhi Fizicheskikh Nauk **171** (8) 801 – 826 (2001)
Translated by E Yankovsky; edited by S N Gorin

fabricate microelectronics devices. The present review puts together and analyzes the knowledge in this area of research gathered in the last few years by scientists from various countries, knowledge that still remains scattered in numerous scientific publications. One can only hope this review will have an impact on the scientists that wish to focus on new avenues of research in solid state physics and on designers of new devices who, after reading this review, will gain a new understanding of the picture, still incomplete, of the properties of the β-SiC(100) surface and of ideas that can be used in various areas of technology.

2. General characterization of silicon carbide

The research of Yu M Tairov and coworkers at the Electrotechnical Institute (St. Petersburg, Russia) and of A O Konstantinov and coworkers at the Ioffe Physicotechnical Institute of the Russian Academy of Sciences (St. Petersburg, Russia) contributed greatly to the development of the technology of growing silicon carbide crystals and to the study of the bulk properties of these crystals [1].

Silicon carbide (SiC) is a wide-bandgap semiconductor that contains 50% silicon atoms and 50% carbon atoms. Today, more than 200 polytypes of SiC are known. These polytypes differ in the order of alternation of double Si – C layers. In each polytype the atoms of one type are centers of tetrahedrons whose vertices contain four atoms of the other type (Fig. 1). There are many hexagonal phases (2H, 4H, 6H, etc.) grouped under the generic name α-SiC. The 4H and 6H phases are the ones most often encountered in the literature, and they are characterized by the ABCB – ABCB and ABCACB – ABCACB alternations of double Si – C layers, respectively. The 2H phase has the ideal classical hexagonal structure of wurtzite (AB – AB).

Our topic will be the surface of the cubic phase (often denoted β-SiC or 3C-SiC), which is characterized by the ABC – ABC layer alternation. This type of SiC exists in the form of very small (several cubic millimeters) bulk crystals and is of poor quality (with a substantial number of defects in comparison to the massive α-SiC crystals). Cubic silicon carbide also exists in the form of thin layers (or films) grown on silicon substrates. These are high-quality single-crystal layers that reach several micrometers in thickness and 100 mm in diameter. The present review is devoted to the structure and properties of the surface of such crystalline layers.

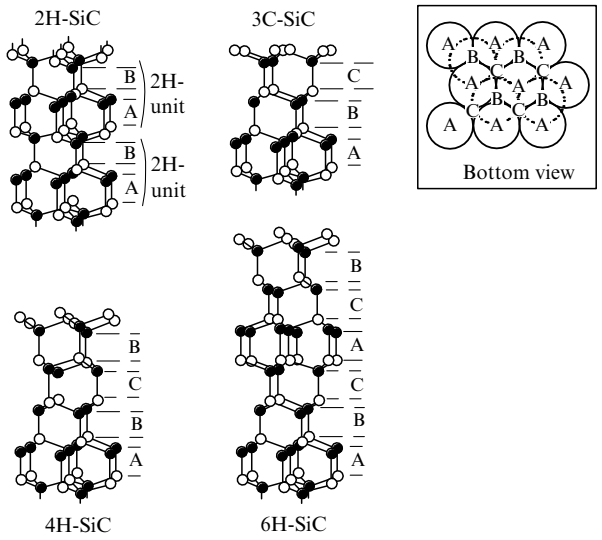

Figure 1. Sequence of double planes of SiC in 2H, 3C, 4H, and 6H polytypes of silicon carbide.

β-SiC has the zinc blende (sphalerite) structure (Fig. 2). This means that its lattice consists of two face-centered lattices shifted in relation to each other in the direction of the cube's diagonal by one-quarter of the diagonal's length. Here, one lattice consists of silicon atoms and the other of carbon atoms. In addition, in the direction $\langle 100 \rangle$ cubic silicon carbide is composed of an alternation sequence of silicon and carbon atomic planes. When we are dealing with a perfect crystal, the (100) surface can be formed by only silicon atoms or only carbon atoms.

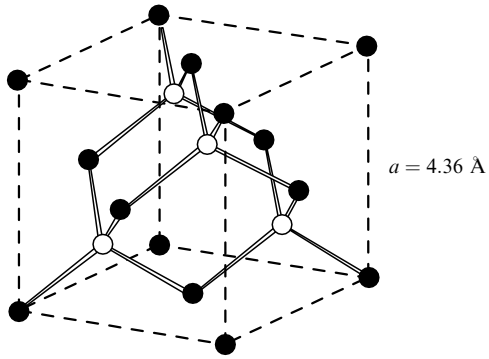

Figure 2. Crystal structure of β-SiC.

Due to the large difference in the electronegativity of the silicon and carbon atoms, SiC is a partially ionic material. This means that a substantial fraction of the charge of silicon atoms is transferred to the carbon atoms. In the bulk, the planes of carbon atoms are negatively charged and those of silicon atoms, positively charged. This feature, combined with the fact that the unit cell of β-SiC is 22% larger than that of diamond and 20% smaller than that of silicon, sets SiC apart from diamond and silicon (which are the ' nearest relations' to SiC).

Silicon carbide possesses a very important property, namely, thanks to the strong Si – C bond, the hardness and wear resistance of SiC are inferior only to those of diamond and cubic boron nitride, with the result that it has long been used in cutting and polishing materials. However, at present it is more often considered as a material for the electronics of the future [2 – 5]. Its wide energy gap makes it possible to use the semiconducting properties of SiC at high temperatures, where the intrinsic conduction of silicon is already quite evident. The high value of the saturation of electron mobility combined with the high breakdown voltage can be used to produce high-power high-frequency devices. At the same time, the thermal conductivity of SiC exceeds that of copper, which in turn facilitates the use of SiC in high-power devices due to its ability to remove the heat produced by the working device. And, finally, the radiation resistance and chemical stability of silicon carbide are also high. These properties make it possible to use SiC under especially severe conditions, e.g., in nuclear reactors or outer space. Table 1 lists some properties of SiC compared to similar properties of silicon.

And yet, since there is no simple production technology, silicon carbide is unable to replace silicon in electronics.

Table 1. Some properties of SiC compared to similar properties of silicon.

Properties	SiC	Si
Energy gap, eV	Direct, 2.4	Indirect, 1.1
Breakdown field, MV/cm	2.0	0.3
Thermal conductivity, W/(cm K)	4.9	1.5
Maximum electron velocity, 10^7 cm/s	2.7	1
Melting point, °C	2830	1400

However, thanks to the considerable effort made in industrial laboratories, especially in Japan and the United States, there is evident progress in this field [2 – 5]. Today silicon carbide is being used to produce high-power high-frequency devices capable of operating at high temperatures and in chemically aggressive media. More than that, SiC is being used as a base for producing electroluminescent devices and detectors of visible and UV radiation. Practically all types of devices can be built on the basis of SiC (diodes, thyristors, field-effect transistors, to name just some). However, due to the high defect density, the production of large SiC-based integrated circuits is still questionable.

Among all the polytypes, the cubic modification of SiC is the most promising for electronics, due to the high electron mobility in this modification. However, at present the most commonly used modification of SiC is the hexagonal, since for this modification there exists a technology for producing large, high-quality SiC crystals. Nevertheless, β-SiC is used in the production of pickups operating above 500 °C. More than that, crystals of cubic silicon carbide serve as perfect substrates for growing some nitrides, which play an important role in optics. And, finally, β-SiC is used to produce multilayer α-SiC/β-SiC type materials. The energy gap of silicon carbide strongly depends on the polytype structure (from 2.4 eV for 3C to 3.3 eV for 4H). Growing crystals with such structures makes it possible to build structures based on homojunctions (of the HEMT type), which can be successfully used at high frequencies and powers. Hence, currently a lot of effort is being put into the development of a technology for fabricating the cubic modification of silicon carbide, which will undoubtedly lead to wide use of this material.

In conclusion of this section, I would like to mention one more property that has been discovered just recently: self-organizing one-dimensional nanoobjects (one-dimensional structures) can form on an SiC(100) surface. Nanostructures are objects consisting of elements whose size, at least in one dimension, is several nanometers or smaller. Generally, nanostructures are divided into three categories: 2D nanostructures (ultrathin mono- and multilayer films), 1D (quantum filaments and linear chains of atoms), and 0D (quantum dots or clusters).

In the last several years the study of the structure of low-dimensional objects and of their properties (electronic, optical, and chemical) has been undergoing a real upsurge [6, 7]. It is extremely difficult to manufacture one-dimensional structures, and for this reason, notwithstanding the effort, they have been studied much less than 0D and 2D structures. Many methods for fabricating one-dimensional structures have been proposed, and each has its advantages and drawbacks.

One method consists in manipulating individual atoms on the substrate and configuring these atoms into one-dimensional objects of the shape required [8]. The invention of the tunneling microscope made this method possible. An advantage of this method is the possibility of producing a structure of any desired shape, but its drawback is the duration of the process, which limits the possibility of producing structures with a large number of atoms.

The newly discovered property of the SiC(100) surface to form self-organizing one-dimensional nanoobjects (one-dimensional structures) has a great advantage, namely, one can rapidly grow large numbers of structures with a great number of atoms in each object. Only a limited number of systems exhibit this property, and it is important that the structures grown on the β-SiC(100) surface manifest unique stability over a broad temperature range.

The majority of papers discussed in the current review deal with research that chiefly involved using high-quality films of SiC with a (100) surface that were grown by Thierry Billon's group at the CEA – LETI laboratory (Grenoble, France) on silicon substrates (100) by chemical vapor deposition (CVD), using SiH_4 and C_3H_8. In addition, some of the samples were grown by André Leycuras at CRHEA (Sophia – Antipolis, France), by Yves Monteil at l'Université Claude Bernard (Lyons I, France), and at Prof. Yu M Tairov's laboratory at the Electrotechnical Institute (St. Petersburg, Russia)

3. β-SiC(100) silicon surface of stoichiometric composition formed by a single monatomic silicon layer

As mentioned earlier, in the ⟨100⟩ direction of the cubic crystal of silicon carbide the atomic planes of silicon and carbon alternate. Hence, an ideal β-SiC(100) surface consists of either silicon atoms or carbon atoms. Naturally, one can prepare a surface rich in silicon (by deposition of an excess amount of Si in vacuum) or in carbon (via silicon desorption). In this section we will discuss the current state of knowledge about the possible structure of the clean surface (100) of cubic silicon carbide. Figure 3 schematically depicts the various structural models proposed for this surface.

Due to the large number of structures (surface reconstructions) revealed in the studies of the clean β-SiC(100) surface, the initial reading of this section may present some difficulties. To make the learning process easier, one can turn to the summary tables in the Appendix (Figures A1 and A2), which list the structures and the methods used to fabricate them.

3.1 2×1 reconstruction of the β-SiC(100) silicon surface of stoichiometric composition observed at room temperature

The first data on the 2 × 1 reconstruction on the β-SiC(100) surface were published in 1985-86 by Dayan [9], Bellina et al. [10], and Kaplan [11]. Using the medium-energy ion scattering (MEIS) method, Hara et al. [12] found that the silicon carbide surface with such a structure consists of a single monolayer of silicon atoms. The (100) surface of silicon carbide resembles the (100) surface of pure silicon at room temperature, which has a 2 × 1 reconstruction consisting of silicon dimers. As the temperature of the silicon crystal is lowered, the surface of the crystal undergoes the Si(100) 2 × 1 – Si(100) c(4 × 2) transition. In this low-temperature surface phase, asymmetric dimers alternate along the dimer chain. It must be immediately noted that the surface of many semiconductors undergoes a reconstruction accompanied by dimer formation. Such transformation reduces the number of

dangling bonds on the surface, since the atoms become grouped into pairs (dimers) and σ bonds parallel to the surface are formed. The remaining dangling bonds usually interact (true, more weakly) with each other and form π bonds, thus reducing the surface energy still further.

Using dynamical diffraction theory to analyze the experimental data on low-energy electron diffraction (LEED), Powers et al. [13] proposed a new model of the β-SiC(100) 2×1 reconstruction, in which the silicon atoms form tightly bound asymmetric dimers slanted to one side and forming long lines in the direction perpendicular to that of the dimer bond.

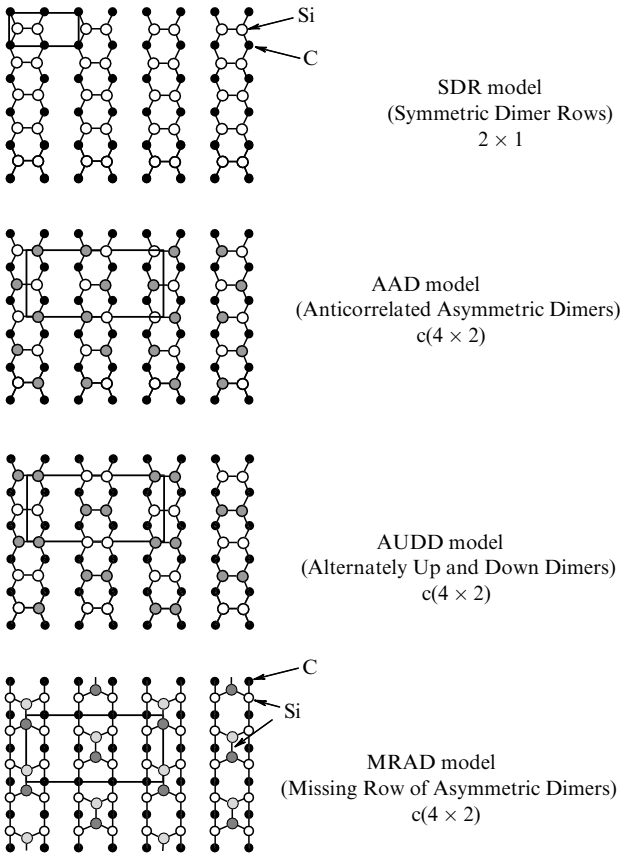

Figure 3. Models of the β-SiC(100) 2×1 and c(4×2) surface reconstructions (according to Ref. [41]).

As for theory, all semiempirical calculations suggest that there is a strong bond in dimers for the 2×1 reconstruction. Some researchers prefer asymmetric dimers [14], while others assume that the dimers are symmetric [15–22]. On the other hand, the first-principles calculations done by Sabisch et al. [23], Käckell et al. [24], and Catellani et al. [25] suggest that the interatomic bond in the dimers is weak and the interatomic distance, large. These calculations contradict the conclusions drawn on the basis of LEED data [13]. However, below we will see that at room temperature the 2×1 reconstruction is probably formed due to contamination of the surface, the presence of a large number of defects, or simply to surface degradation. Actually, this reconstruction exists at $T \geqslant 400\,^{\circ}\mathrm{C}$ (see below), while the main reconstruction inherent in the β-SiC(100) surface at room temperature is c(4×2).

3.2 c(4×2) reconstruction of the β-SiC(100) silicon surface of stoichiometric composition

The other reconstruction of the β-SiC(100) surface, c(4×2), was discovered in 1988–1989 by Kaplan [26]. By analogy with the Si(100) c(4×2), a model was proposed in which the β-SiC(100) c(4×2) surface consists of anticorrelated asymmetric dimers (see Fig. 3).

Since it is very difficult to fabricate this structure in experiments, for a long time the majority of research groups, both experimenters and theoreticians, did not even mention it. Only in 1996 did the first publication concerning the c(4×2) reconstruction appear (see Ref. [27]), and the method used was photoemission from the core level Si_{2p}. The decomposition of the spectrum of this level into three components (two of which are surface components) and the exceedingly large ratio of the sum of intensities of the surface components to the intensity of the bulk component led to the conclusion that the β-SiC(100) surface contains more than one monolayer of silicon atoms.

In that same year, Semond et al. used scanning tunneling microscopy (STM) to study this structure for the first time (see Ref. [28]). They found that the c(4×2) reconstruction is characteristic of the (100) surface with a single monolayer of silicon atoms, while the 2×1 reconstruction appears, apparently, due to contamination of the surface, the presence of a large number of defects, or simply to surface degradation.

The measurements done by this group of researchers [28] were, actually, the first measurements that enabled scientists to directly identify the dimers of silicon on the (100) surface. Combined with theoretical STM image calculations done by a group of researchers headed by Joachim [29], these measurements made it possible to propose one more model of the c(4×2) reconstruction [29]. According to this model, the surface consists of orderly arranged symmetric dimers of silicon atoms. The long-range order dimers are positioned alternately above and below a certain median level. This alternate arrangement is accompanied by a very significant redistribution of charge between neighboring dimers, namely, the dimers that are above the median level have a higher density of occupied states. The model became known as the Alternately Up and Down Dimers (AUDD) model. Somewhat later, Douillard et al. [30] used *ab initio* calculations to corroborate this model; i.e., the alternate arrangement of dimers above and below a median level was established, the charge transfer that was predicted earlier was confirmed, and, finally, it was shown that dimers below the level are shorter than those above the level (2.27 Å and 2.53 Å, respectively) and that the difference in their heights is 0.23 Å. Note, however, that the theoretical STM image calculations done in Ref. [29] predicted a difference in dimer height equal to 0.1 Å. In 1998, a group of researchers headed by Galli (see Ref. [31]) performed new *ab initio* calculations for this surface. First, the previous calculations done by the same group (see Ref. [25]) were corroborated. They also found that in the absence of a stressed state the most stable structure is 2×1, which consists of long dimers with weak bonds. Generally speaking, the surface experiences stresses, but a large number of defects (dimer vacancies) diminishes these stresses and stabilizes the 2×1 reconstruction. However, the same calculations showed that in the presence of a certain excess stress applied to the surface, the latter demonstrates the c(4×2) reconstruction and supports the AUDD model. With the method of growing films of cubic silicon carbide in mind, one can easily understand that it is practically impossible to

avoid the stressed state. It is the stresses that stabilize the c(4 × 2) reconstruction. This group of researchers also did theoretical STM image calculations (in the mode of occupied states), with the results being in good agreement with the images obtained by Semond [28].

A remark concerning the state of stress is in order. The crystal structure of β-SiC is actually the same as that of silicon, but the unit cell parameter of SiC is 20% smaller than that of silicon. This enormous difference in the unit cell parameters leads to a highly stressed state in the film. To balance this difference, a carbon layer is deposited onto the silicon substrate in advance. Nevertheless, since the growth takes place at high temperatures and the difference in the thermal expansion coefficients of Si and SiC is large, the film is always in a highly stressed state (even if the film is only several microns thick).

In 1998, another group of researchers proposed a new model of the c(4 × 2) reconstruction on the basis of *ab initio* calculations [32]. This model, called MRAD (Missing Row Asymmetric Dimers) assumes that there are 1.5 monolayers of silicon on the (100) surface. (In the AUDD there is a single monolayer of silicon atoms.) This value (1.5 monolayers) appears to be very strange [12, 33] and does not correspond to the existing experimental data [34].

From the section that follows, where we discuss the study of the c(4 × 2) surface by Si_{2p} core-level photoemission spectroscopy, we will see that the AUDD method is preferable to the MRAD method.

3.2.1 The study of the c(4 × 2) surface by photoemission spectroscopy. Prior to the results presented in this section, there was only one publication devoted to the c(4 × 2) reconstruction (see Ref. [27]). The researcher used photoemission spectroscopy to study the core level Si_{2p}. The drawbacks of this approach are as follows:

(1) at that time (1996), the preparation of a surface with a given type of structure could not be properly monitored;

(2) only a single value of the photon energy was used;

(3) the energy resolution was no better than 0.4 eV.

In her study, Shek [27] decomposed the spectrum into three components: one bulk component and two surface components. The ratio of the sum of intensities of the surface components to the intensity of the bulk component prompted Shek to conclude that the content of silicon atoms on the outer surface exceeds one monolayer. Pollmann and collaborators used this conclusion to develop the MRAD model [32] (see above).

Recently the validity of this or that model was verified by applying Si_{2p} core-level photoemission spectroscopy to study in detail the c(4 × 2) reconstruction [35]. This research was conducted using the SU3 line of the Super-ACO source of synchrotron radiation (L.U.R.E Orsay). A broad spectrum of photon energies was used in order to obtain core-level spectra in modes of enhanced surface and bulk sensitivities and in intermediate-sensitivity modes. The energy resolution was 150 meV. The structure of the surface was found to correspond to a single-domain c(4 × 2) reconstruction, which was regularly monitored through the presence of sharp reflections in LEED.

The Si_{2p} core-level spectra were obtained for photon energies ranging from 115 to 135 eV. It was found that the intensity of the peak in the region of lowest binding energies increases with photon energy and reaches its maximum at a photon energy of 130 eV, which in turn also corresponds to the maximum surface sensitivity (the ratio of the signal from the surface to that from the bulk) for the case of electron excitation from the Si_{2p} level. On the other hand, the intensity of the peak in the region of high binding energies increases as the photon energy decreases down to 115 eV. Such photon energy is used in silicon studies to investigate the atoms in the bulk. The central part of the spectrum retains its high intensity over the entire range of photon energies and, therefore, contains contributions both from surface atoms and from bulk atoms.

For a better understanding of the nature of the spectra, they were decomposed into Voigt [36] doublets. The parameters adopted by the researchers were those usually used in processing the experimental spectra of Si_{2p} [37]: the Lorentz width was 85 meV and the spin–orbit splitting 602 meV. The peak S1 located far from all other peaks, made it possible to estimate the Gaussian width of the surface components of the spectrum at 0.55 eV. For the bulk peak, the researchers used the Gaussian distribution width of approximately 0.6 eV. This is three times larger than the value usually used in studies of single-crystal silicon but is in good agreement with the results of other SiC photoemission studies [38, 39].

Figure 4 depicts the spectra for three values of the photon energy and their decomposition into components. This is the only method that makes it possible to decompose the spectra for all the photon energies in question; as we will shortly see, this decomposition has a physical explanation. Table 2 lists the results of the decomposition. The behavior of the SB2 component is similar to that of the bulk component B, while the behavior of the SB1 component (intermediate between the bulk and surface components) more resembles the behavior of the bulk component at low photon energies and that of the surface component, at higher photon energies.

Table 2. Results of decomposition of the Si_{2p} core-level spectra into components obtained for photon energies ranging from 115 to 135 eV.

Component	Binding energy, eV	Position relative to peak B, eV	Gaussian width, eV
S1	~99.8	−1.43	0.55
S2	~100.66	−0.54	0.55
SB1	~100.8	−0.40	0.55
B	~101.2		0.60
SB2	~101.51	+0.31	0.55

To determine the physical origin of each component, the researchers studied the photon-energy dependence of the relative component intensities. It was found that the intensities of the S1 and S2 components are practically the same for every energy in the entire range of photon energies in question. The intensity of these components increases as the photon energy grows from 115 to 130 eV and somewhat decreases at 135 eV. Such a dependence is in very good agreement with the behavior of the surface components and is related to the evolution of the mean free path of the electrons excited from the Si_{2p} level in the same range of photon energies. Thus, the S1 and S2 peaks can be identified as the surface components. The fact that the behavior of the B component is just the opposite makes it possible to identify the B peak as the bulk component.

To better understand the SB1 and SB2 components, the researchers studied the behavior of all the components with the intensities normalized to the total intensity of the surface

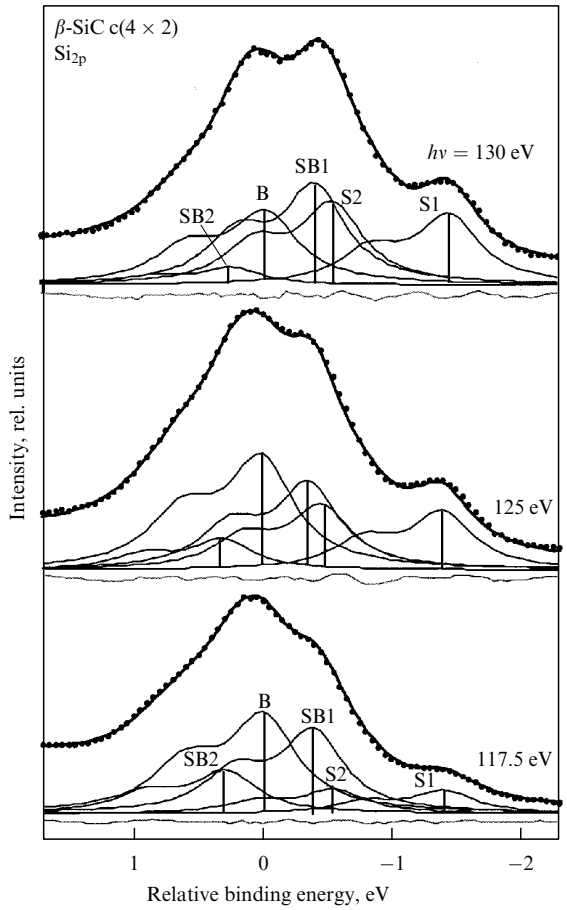

Figure 4. Decomposition of Si_{2p} photoemission spectra of the c(4 × 2) reconstruction for three energies of the exciting photons: $h\nu = 130$, 125, and 117.5 eV. The spectrum at 130 eV is the most sensitive to the surface, while that at 117.5 is the most sensitive to the bulk [35].

components S1 and S2. Figure 4 suggests that all the components except S1 and S2 behave like bulk components; such behavior is most evident for the B and SB2 components and less evident for the SB1 component.

Finally, to quantitatively estimate the probing depth, the researchers used the relative intensities for determining the mean free paths of electrons at each energy. To this end it was assumed that the total intensity $I_{S1} + I_{S2}$ corresponds to the emission from a single outer (surface) monolayer of silicon atoms. More than that, it was assumed that the measured intensity decreases exponentially with increasing distance from the surface to the depth at which the atoms emit electrons (by the definition of the mean free path). In all measurements, the angle of emission amounted to 45° with respect to the normal to the surface. Then the ratio of the intensity I_n of electrons emitted by the nth atomic plane at a distance $d \times n$ from the surface, to the intensity I_0 of photoelectrons from the first monolayer of surface atoms is given by the expression

$$\frac{I_n}{I_0} = \exp\left(-\frac{1.414nd}{\lambda}\right),$$

where λ is the mean free path of electrons for a given energy, and $d = 2.2$ Å is the distance between the neighboring silicon planes.

Also, the ratio of the sum of intensities from all planes except the outer one to the intensity from the outer plane is

$$\sum_{n=1}^{\infty} \frac{I_n}{I_0} = \frac{\exp(-1.414d/\lambda)}{1 - \exp(-1.414d/\lambda)}.$$

Table 3 lists the results of these calculations, namely, the electron mean free path λ as a function of the relative bulk/surface intensity obtained by decomposition. The estimated value of the electron mean free path varies from 6 to 21 Å as the photon energy varies from 135 to 115 eV. Note that the larger the electron mean free path in the solid, the greater the depth from which the electrons can be brought out of the crystal without loss of energy and hence the greater the information about the bulk carried by the spectrum (one speaks of the 'higher bulk sensitivity'). This dependence agrees perfectly with the 'universal curve.' Note once more that the highest surface sensitivity proves to be that for electrons excited by photons with an energy equal to 130 eV. Thus, these experimental results serve as direct quantitative proof of the earlier assumption that the S1 and S2 components represent the emission from atoms that are directly at the surface and form a single atomic plane. Hence, there is reason to believe that the S1 and S2 components originate from the dimers positioned above and below a certain median level in the AUDD model of the c(4 × 2) superstructure. The fact that the intensities of S1 and S2 are equal is an indication that each of these components originates from an equal number of atoms, while the large difference in the position of these components on the energy scale is an indication of a redistribution of charge between the raised and lowered dimers. Note the analogy with the Si(100) c(4 × 2) surface, where the two surface components, separated by 0.55 eV on the energy scale [27], originate (as has been established) from the raised and lowered atoms of the asymmetric dimers constituting the surface. In this case, charge is transferred from the lower atoms to the higher atoms, while in the case of SiC atoms the charge transfer is from the lower dimers to the higher dimers. This assumption is in perfect agreement with the STM data, which indicate a considerable difference between the charge states of the two dimer types.

Table 3. Electron mean free path λ as a function of the relative bulk/surface intensity obtained through peak decomposition.

Photon energy, eV	Relative intensity $(I_B + I_{SB1} + I_{SB2})/(I_{S1} + I_{S2})$	Estimated mean free path λ, Å
115	6.35	21.3
117.5	5.15	17.5
120	4	13.9
122.5	2.5	9.2
125	1.95	7.5
127.5	1.55	6.2
130	1.45	5.9
135	2.75	10

Note that in 1998 Lu et al. [32] proposed a new model of the c(4 × 2) reconstruction based on *ab initio* calculations. This MRAD model assumes that there are 1.5 monolayers of silicon on the outer surface instead of only one silicon monolayer in the AUDD model. Remaining within this MRAD model, one can assume that the S1 and S2 components originate from surface dimers that are above or below a certain median level, while the SB1 or SB1 + SB2

components originate from the Si atoms belonging to the first, completely occupied, plane. Then the intensity of SB1 + SB2 must be exactly twice the intensity of S1 + S2. This result, however, does not agree with the data on the behavior of the components whose intensity is normalized to the total intensity of the surface components S1 and S2 (for the photon energy corresponding to the maximum surface sensitivity, $I_{SB1} + I_{SB2} \sim I_{S1} + I_{S2}$). More than that, to correspond to the MRAD model, the decomposition must contain two other components of equal intensity that would correspond to the atoms belonging to the raised or lowered dimers.

What remains to be discussed is the origin of the SB1 and SB2 components in the AUDD model. As noted earlier, these components correspond to emission from the silicon atoms in the bulk. Nevertheless, even at 115 eV the probing depth remains moderate (22 Å, which amounts to a dozen atomic planes of silicon). Hence, we must assume that according to the AUDD model a superstructure not only triggers a transformation in the surface layer of atoms but also affects the arrangement of the atoms in several atomic planes near the surface. Probably, the strong redistribution of charge observed in the surface layer induces a redistribution of charge in the planes just under the surface. For instance, theoretical calculations for silicon have shown (see Ref. [40]) that in the case of the c(4 × 2) reconstruction the charges in the atomic arrangement and electronic structure extend to at least three atomic planes lying below the first surface monolayer. Probably, SiC should be expected to behave in a similar manner, since the crystal lattice of SiC is partially ionic. In the bulk, each atomic plane of silicon transfers a fraction of its charge to two neighboring atomic planes of carbon, while the outer atomic plane of silicon can transfer a fraction of its charge only to one carbon plane. Thus, the carbon plane just below the surface silicon plane carries a charge different from that of any inner carbon plane. This also implies that the silicon plane positioned just below the first carbon plane also differs from the other silicon planes in the bulk. Thus, calculations that incorporate cluster models must include a rather large number of atomic planes so as to take into account the general structural changes caused by the surface's transformation.

In conclusion of this section, we would like to note once more that in Ref. [35] the decomposition of the spectrum of the core level Si_{2p} of the c(4 × 2) surface of cubic silicon carbide is into five components, two of which correspond to surface silicon dimers positioned raised and lowered in relation to a certain median level. The other two components (excluding the bulk component) reflect the transformation of the atomic silicon layer that are farther from the surface. The results of these investigations are in satisfactory agreement with the AUDD model. More than that, spectroscopic identification of the alternation of up and down dimers proved very important for studies of chemical reactions of this surface with adsorbates [41].

In the section that follows, we describe one more unusual property of the silicon-terminated β-SiC(100) surface of stoichiometric composition: at $T \sim 400\,^{\circ}C$, there exists a semiconducting c(4 × 2) ⇔ metallic (2 × 1) reversible phase transition. More than that, it was found that the 2 × 1 superstructure can emerge not only due to defects but can even exist independently at elevated temperatures ($T > 400\,^{\circ}C$).

3.3 Reversible phase transition c(4 × 2) ⇔ (2 × 1) on the β-SiC(100) surface

3.3.1 Temperature-induced c4 × 2) ⇔ (2 × 1) phase transition on the β-SiC(100) surface. As noted above, earlier it was assumed that the β-SiC(100) 2 × 1 reconstruction can exist only as a result of contamination or the presence of defects on the c(4 × 2) surface. It was found, however, that at elevated temperatures this structure can exist independently [43, 43]. The experiments were performed using an Omicron VT-STM scanning tunneling microscope, which operates at temperatures ranging from −230 °C to +900 °C.

Moreover, measurements were performed using a VG angle-resolved spectrometer equipped with a hemispherical electron analyzer. The surface structure was also monitored by LEED. Figure 5a depicts the 100 × 100 Å STM topographs of the β-SiC(100) surface at room temperature, typical

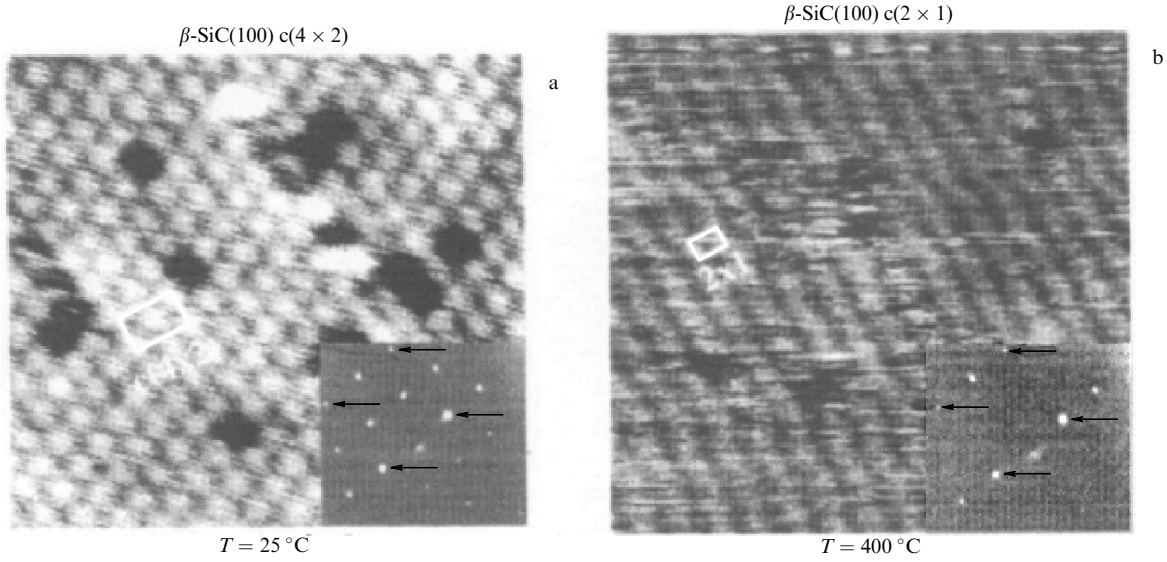

Figure 5. 100 × 100 Å STM topographs (filled states) of (a) β-SiC(100) c(4 × 2) at 25 °C and (b) β-SiC(100) 2 × 1 at 400 °C; the tip bias was $V = +3.2$ V at a tunneling current $I = 0.12$ nA. The corresponding LEED diagrams ($E_p = 60$ eV) are in the lower right corners, with the arrows pointing to the (1 × 1) reflections [42].

of the c(4 × 2) reconstruction. The corresponding LEED diagram is given in the lower right corner. Figure 5b depicts a similar STM topograph of the same sample after it was heated to 400 °C. The topograph is typical of the 2 × 1 reconstruction. Earlier such a topograph was obtained at room temperature with a poorly prepared surface. The LEED diagram, suggesting that this is indeed a 2 × 1 reconstruction, is depicted in the lower right corner of the STM topograph. The cooling of the sample to 25 °C and then a repeated heating to 400 °C resulted, in a reversible manner, in topographs identical to those depicted in Figs 5a and 5b, respectively.

To compare the characteristics of these structures, STS was done at approximately one thousand points, both at 25 °C and 400 °C. The averaged current – voltage curves of these measurements are depicted in Fig. 6. The c(4 × 2) current – voltage curve recorded at 25 °C (curve *a*) exhibits a horizontal section of about 1.7-V long, clearly indicating the semiconducting nature of the surface.

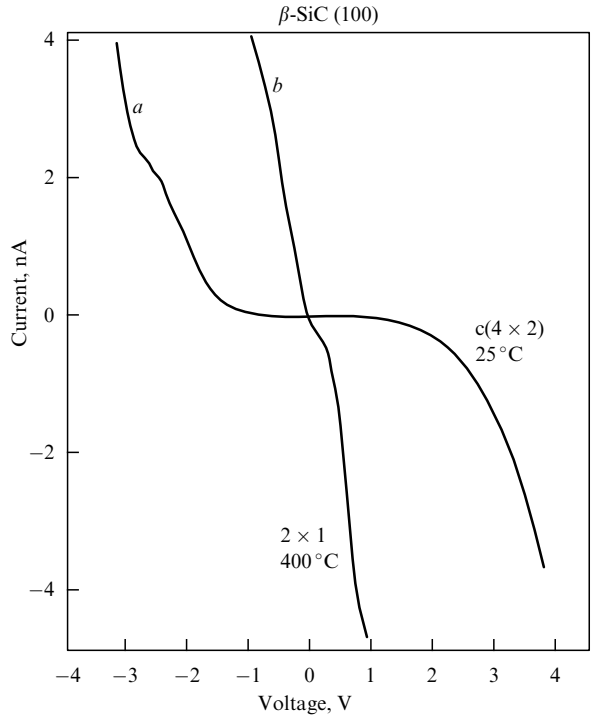

Figure 6. Current – voltage characteristics obtained by the STS method for β-SiC(100) c(4 × 2) at 25 °C (curve *a*) and for β-SiC(100) 2 × 1 at 400 °C (curve *b*). Such curves represent an average of one thousand current–voltage characteristics recorded all over the 100 × 100 Å surface by equal steps. The sample was grounded [42].

Note that in the semiconductor's bulk the fundamental gap amounts to 2.3 eV. On the other hand, the 2 × 1 current – voltage curve recorded at 400 °C (curve *b*) is almost linear and does not have any measurable gap, which points to the metallic nature of this structure.

Additional information about the phase transition was extracted from studies of the electronic structure of the c(4 × 2) surface by the angle-resolved photoemission spectroscopy (ARPES) method. The peak in the photoemission spectra discovered approximately 1.3 eV below the Fermi level (E_F), characteristic of a c(4 × 2) reconstruction, reversibly vanished and appeared as the temperature varied in the 25 – 400 °C range. The disappearance of the peak at elevated temperatures proves that the c(4 × 2) reconstruction undergoes a phase transition.

Figure 7 is a schematic of the superstructures in question. Probably, at 400 °C (the 2 × 1 reconstruction) the lines connecting the neighboring atoms in a dimer are parallel to the surface and all dimers are on the same level. By analogy with the calculations done by Lu et al. [44] for exactly the same configuration of dimers on the Si(100) 2 × 1 surface, the 2 × 1 superstructure discovered in this work must be metallic. Cooling the sample will, probably, lead to a Peierls transition and, as a result, to formation of a gap at the Fermi level. Here, in accordance with the findings of Catellani et al. [45], the lines connecting neighboring atoms in a dimer are parallel to the surface, while along a dimer chain there is 'up-down' alternation.

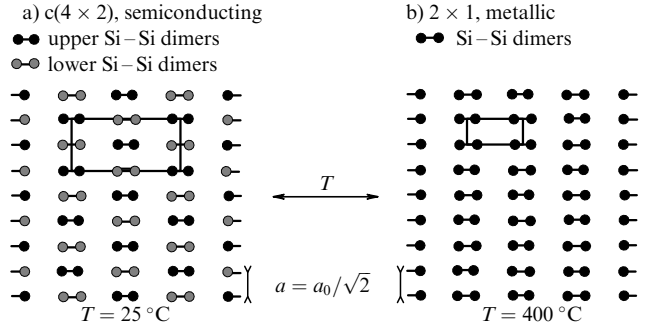

Figure 7. Reversible phase transition on the β-SiC(100) surface from the c(4 × 2) reconstruction, which has an alternately up and down dimer (AUDD) sequence in a row, to the 2 × 1 reconstruction, whose dimers are on the same level. The corresponding unit cells are also given [42].

3.3.2 Reversible phase transition c(4 × 2) ⇔ (2 × 1) on the β-SiC(100) surface caused by adsorption of residual gases. We note once more that until recently it has been assumed that the silicon-terminated β-SiC(100) surface of stoichiometric composition exhibits a 2 × 1 reconstruction, by analogy with Si(100) and Ge(100), with this fact corroborated both theoretically and experimentally. However, not so long ago it was found, through LEED measurements, that these experimental data were obtained for low-quality surfaces, i.e., surfaces with a large number of defects and/or contaminations [3 – 5, 28, 46 – 49]. Note that in 1991 Stroscio and Eigler [8] and Iijima [50] hypothesized that this could be the case. Actually, it appears that a carefully prepared surface has a c(4 × 2) structure at room temperature. More than that, this structure is not similar to the low-temperature phase on silicon and germanium surfaces. In contrast to Si and Ge, this structure is an alternation of up and down symmetric dimers (parallel to the surface), or the AUDD model [28, 29]. Below, we will see that the results of calculations also speak in favor of this model [50, 51].

However, except for the LEED data and the assumptions made by Stroscio and Eigler [8] and Iijima [50], before the paper by Douilard et al. [52] appeared, there were no direct indications that the commonly prepared surface reconstruction 2 × 1, an object of many studies at room temperature, is actually characteristic of a poorly prepared surface. In this section, we will see how the STM method has been used to directly prove that the adsorption of a minute quantity of

residual gases in a high-vacuum actually leads to the reversible phase transition $c(4 \times 2) \Leftrightarrow (2 \times 1)$. This investigation has simultaneously proved that the $c(4 \times 2)$ reconstruction is very sensitive to adsorption of residual gases [52]. The measurements were done with an Omicron VT-STM scanning tunneling microscope at room temperature. The pressure in the spectrometer was maintained at 4×10^{-11} Torr. Additional monitoring of the surface state was done by the LEED method.

Figure 8a depicts a 150×150 Å STM image of the atomically clean β-SiC(100) surface of stoichiometric composition with the $c(4 \times 2)$ reconstruction. The image was recorded at room temperature with all electronic states filled. The diffraction pattern of this surface has been placed in the upper left corner of the image. This pattern was obtained by the LEED method and also corroborates the presence of the $c(4 \times 2)$ reconstruction. The STM image is a system of bright spots that form a pseudohexagonal pattern similar to that obtained earlier by Semond et al. [28, 29], who associated it with the silicon dimers positioned above a median level (the AUDD model). By simulating STM images, Semond et al. [28, 29] also established that despite the small difference in the heights of the alternating dimers (0.1 Å) the dimers positioned below the median level are 'invisible' to the probing needle in the STM method. To determine the effect of residual gases on the $c(4 \times 2)$ reconstruction, the sample was left for 14 h in the ultrahigh-vacuum spectrometer with the pressure of residual gases (mainly H_2) being approximately 5×10^{-11} Torr. The 150×150 Å STM image of this surface obtained in the filled-states mode is depicted in Fig. 8b. We see that the most striking difference that sets this surface apart from the initial one is the absence of the characteristic centered pseudohexagon. Instead we observe a set of closely spaced parallel rows. The periodicity in the direction perpendicular to the rows amounts to 6.2 Å, which is approximately twice the parameter of the unreconstructed surface (3.08 Å). The resolution in the direction of the rows was insufficient to detect any periodicity. In addition to the STM topograph, in the upper left corner in Fig. 8b there is also a sharp diffraction pattern, obtained by the LEED method, which corresponds to the same surface. This photograph is a clear indication of the presence of a 2×1 reconstruction detected by the STM method. The exposure of this surface to an atmosphere of residual gases corresponds to 2.5 L (1 L$= 10^{-6}$ Torr s). However, there could be another explanation of these results. Let us assume that actually it was not the surface that underwent considerable transformation as a result of a 14-h exposure but that simply the tungsten probing needle became contaminated, which made it impossible to achieve atomic resolution of the surface. To check this assumption, the researchers heated the sample to 900 °C and maintained that temperature for 30 s. Such heating removes the adsorbate from the sample surface and at the same time does not lead to silicon desorption, thus leaving the stoichiometry of the surface intact. The surface of the needle was not subjected to such heating and therefore remained unaltered. Figure 8c depicts a 150×150 Å STM image of the sample surface after the additional heating was carried out (it also was taken in the filled-states mode). Clearly visible is a $c(4 \times 2)$ reconstruction, which we have already seen in Fig. 8a representing the atomically clean surface. The corresponding photograph of a sharp diffraction pattern obtained by the LEED method has also been placed in the upper left corner in Fig. 8c. Thus, Douilard et al. [52] have shown that on the silicon-terminated

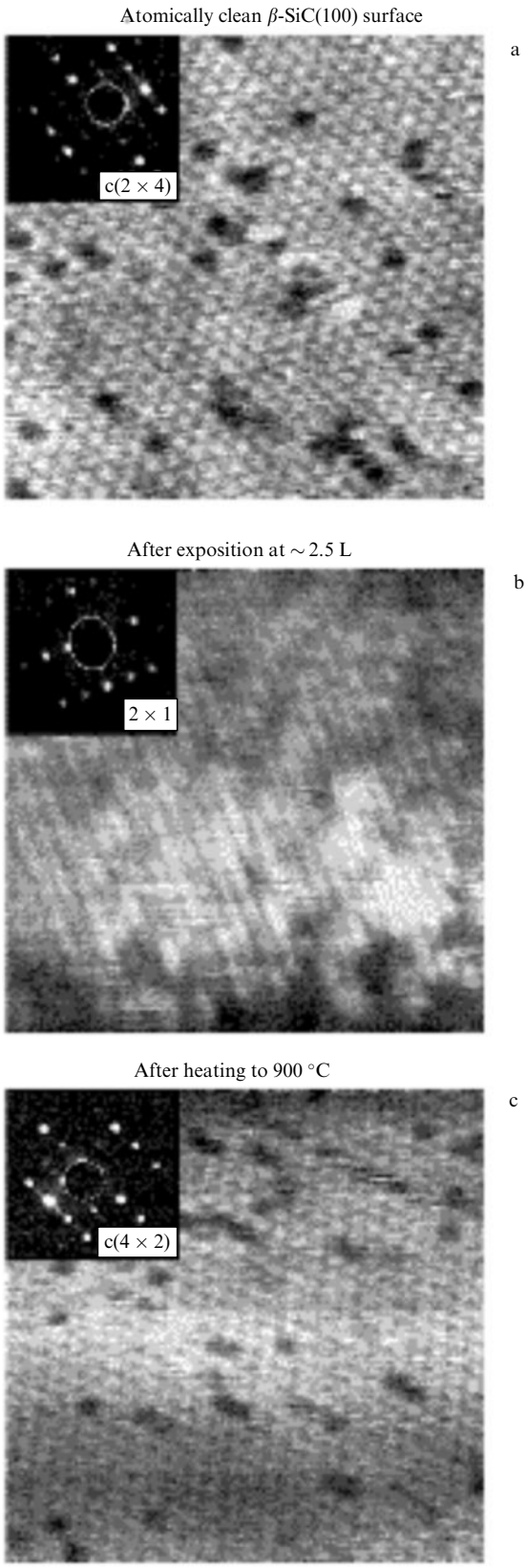

Figure 8. 150×150 Å STM topographs of (a) an atomically clean β-SiC(100) $c(4 \times 2)$ surface; (b) β-SiC(100) 2×1 obtained after exposition of the structure (a) for 14 h in a 5×10^{-11} Torr vacuum; (c) surface (b) after rapid heating to 900 °C. The topographs were registered at room temperature with all electronic states filled. The LEED photographs corroborating the presence of structures have been placed in the upper left corners of the corresponding topographs [52].

β-SiC(100) surface of stoichiometric composition at room temperature a reversible phase transition $c(4 \times 2) \Leftrightarrow (2 \times 1)$ occurs caused by adsorption – desorption of residual gases in the ultrahigh-vacuum spectrometer. At the same time, the researchers directly proved that the formation of a surface superstructure 2×1 is the result of surface contamination, as earlier LEED experiments suggested [3 – 5, 28, 46 – 49]. This explains the fact that for a long time researchers were unable to detect the $c(4 \times 2)$ reconstruction and assumed that at room temperature the 2×1 reconstruction was the main one for the silicon-terminated β-SiC(100) surface of stoichiometric composition. More than that, it became clear why it is so difficult to study the $c(4 \times 2)$ superstructure compared to other reconstructions of the β-SiC(100) surface. Since the dominating component of residual gases is molecular hydrogen, it is, probably, responsible for the changes in surface structure.

Thus, the surface structure can undergo significant changes caused by small adsorption. The adsorbate substantially alters the local charge distribution, which results in a transformation from the alternate up-and-down dimer pattern to the pattern in which all the dimers are positioned at the same height. Removing this gaseous adsorbate from the surface by heating the surface to 900 °C for a short time restores the original charge distribution between neighboring dimers and the original superstructure characteristic of an atomically clean surface of stoichiometric composition. Note that the nature of the phenomenon caused by the adsorption of residual gases is quite different from that of the temperature-induced reversible phase transition $c(4 \times 2) \Leftrightarrow (2 \times 1)$ discussed earlier.

3.4 One-dimensional nature of the metallic conduction of the 2×1 superstructure on the β-SiC(100) surface

In Section 3.3.1 we described how STS can be used to show that the 2×1 reconstruction of the (100) surface exhibits metallic conduction. However, usually the STS results alone are insufficient for unambiguously proving that the properties of the surface are indeed metallic. One of the main methods to solve this problem is photoemission spectroscopy (PES). Enriquez et al. [53] used the PES method to conduct, near the Fermi level, comparative investigations of the valence-band electronic structure of the β-SiC(100) $c(4 \times 2)$ surface at 25 °C (prior to the phase transition) and of the β-SiC(100) 2×1 surface at $T > 400$ °C (after the phase transition). Below, we will see how the PES data near the Fermi level unambiguously demonstrate the presence of emission and hence of metallic conduction. Detailed analysis (see Ref. [51]) has shown that one of the most probable mechanisms of the surface conduction of the 2×1 reconstruction is one-dimensional conduction. Comparative analysis of core-level spectra before and after the phase transition also corroborates this conclusion. The possible quasi-one-dimensional conduction of the β-SiC(100) surfaces terminated by an atomic silicon plane may be the reason the properties of this surface differ so dramatically from the those of the similar (at first glance) Si(100) surface.

Enriquez et al. [53] conducted their photoemission studies using the VUV line of the ELETTRA source (Triest, Italy) of synchrotron radiation and an SGM monochromator. The emitted electrons were analyzed with an angle-resolved spherical electrostatic analyzer. The energy resolution (together with thermal broadening) was 200 meV, while the angular resolution was $\pm 0.5°$. Since the temperature at which the 2×1 reconstruction can be studied must be higher than 400 °C, a method for pulsed heating of the sample had to be developed. Indeed, to heat the sample by direct current, a voltage must be applied to the sample. As a result, a potential gradient emerges on the section of the surface from which electrons are emitted (and are then directed into the analyzer). Thus, with the sample length being roughly 10 mm, the size of the analyzed section being roughly 1 mm, and the voltage across the sample being roughly 10 V, the kinetic energies of the emitted electrons may differ by 1 eV for different points of the analyzed section. If one allows for the fact that even at high temperatures of the sample the energy resolution is roughly 200 meV, it becomes clear that no measurements are possible since the actual energy resolution in this case exceeds 1000 meV. The pulsed heating method developed and used in these measurements [53] consists in the following. A pulsed current of rectangular shape in the current – time coordinates is sent through the sample. The pulse length is 50 ms, which is the time during which the sample gets heated. For the subsequent 50 ms the sample is grounded, and that is when the emitted electrons are collected and analyzed. Due to the large mass of the sample, the sample temperature remains practically unchanged.

As noted earlier, valence-band photoemission spectroscopy is a unique instrument for determining the type of conduction. For two- and three-dimensional systems, when the surface exhibits metallic properties, near the Fermi level in the valence-band spectra there can be observed a Fermi step, which is a characteristic feature of such properties. Figure 9 depicts the photoemission spectra at the $\bar{\Gamma}$ point of the surface Brillouin zone near the Fermi level for two structures: $c(4 \times 2)$

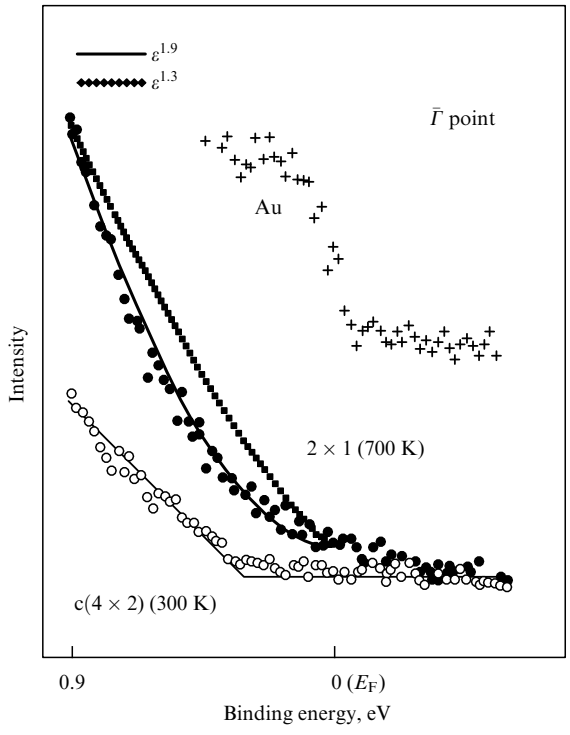

Figure 9. Photoemission spectra at the $\bar{\Gamma}$ point of the surface Brillouin zone near the Fermi level for two reconstructions: $c(4 \times 2)$ at 300 K and 2×1 at 700 K. The solid curve represents the approximation by a power-law function with the exponent equal to 1.9. The data on the gold foil in electric contact with the sample are depicted in the upper half of the figure. The photon energy is $h\nu = 18.9$ eV [53].

at 25 °C and 2 × 1 at 400 °C. The spectrum corresponding to the first reconstruction exhibits a distinct gap near E_F, thus proving the semiconducting nature of the surface. The gap disappears after heating, and we observe the gradual emergence of emission near E_F. Thus, at $T > 400$ °C the surface ceases to be semiconducting, but at the same time no characteristic metallic step is observed. The same figure depicts the spectrum, taken under the same experimental conditions, of a gold foil that is in electric contact with the sample. There is clearly a metallic step, whose middle points to the position of E_F and whose width makes it possible to determine the instrumental broadening. But even if we allow for the thermal broadening caused by the rise in the sample temperature from room temperature to 400 °C, we still do not get the shape of the spectrum obtained for the 2 × 1 reconstruction.

Thus, we may conclude that the behavior of the electron density near E_F differs from that characteristic of a Fermi liquid. There are, probably, not enough experimental data to draw far-reaching fundamental conclusions, but still we will try to give a possible explanation of the observed phenomenon.

A characteristic feature of Fermi liquids is that the elementary excitations are independent, obeying Fermi statistics. This results in a 'metallic' step appearing near E_F in the spectra. However, when there is strong electron–electron coupling, as is the case with, say, low-dimensional systems, the behavior of the Fermi liquid may not correspond to that of the electron system. In the one-dimensional case, the behavior of a system of strongly correlated electrons can be related to the Luttinger-liquid model [54–56]. The excitations of independent quasiparticles are replaced by collective excitations with spin–charge splitting. In this case the theory predicts a power-law dependence of the photoemission intensity $(E - E_F)^{\alpha}$ near the Fermi level, with the exponent α directly related to the strength of the correlation in the electron system [55, 56].

In Ref. [53], the spectrum of the β-SiC(100) 2 × 1 surface, measured near the Fermi level, was approximated by a power-law function. This result suggests that a one-dimensional model of an electron liquid is functional and corresponds to the Luttinger-liquid model.

Thus, one of the possible explanations of the observed behavior of the electron density near E_F is as follows. Apparently, a quasi-one-dimensional strongly correlated system of electrons forms on the β-SiC(100) surface at $T > 400$ °C. Similar behavior of the electron density (with a power-law density in photoemission spectra near the Fermi level) is observed in the well-known quasi-one-dimensional materials, such as organic conductors [57] and inorganic materials with a chainlike structure, e.g., $(TaSe_4)_2I$, $K_{0.3}MoO_3$ or $BaVS_3$ [56, 58, 59]. Dardel et al. [57] used the Luttinger-liquid model to describe the behavior of the electron systems of these materials.

However, in contrast to these materials, in the case of β-SiC(100), a quasi-one-dimensional electron system probably resides in the outer monatomic layer of the wide-gap semiconductor. The quasi-one-dimensional properties of the β-SiC(100) surface are in no way related to the properties of the bulk material under the surface. More than that, these properties are not related to metallic filaments that may be formed on the surface as a result of deposition of metallic atoms. The fact that the surface is quasi-one-dimensional could be explained by the behavior of the electron system of the interacting Si–Si dimers belonging to the same dimer chain. Note that on the surface the size of the period along the chain amounts to 3.08 Å, while in the direction perpendicular to the chain it is 6.16 Å. Hence, obviously, there is a strong overlap of the wave functions of dimers belonging to the same row (chain) and a very weak overlap of the wave functions of dimers belonging to different rows (chains).

If near the Fermi level the behavior of the photoelectron spectra registered in an integrated-over-angles mode is described by a power law, the strength of the correlation can be estimated by the exponent α. Enriquez et al. [53] approximated the spectra by power-law functions with the exponents being $\alpha = 1.9$ for the Γ point and $\alpha = 1.3$ for the J point of the surface Brillouin zone. In the Luttinger-liquid model, these two values correspond to very strong electron–electron correlation. For instance, in quasi-one-dimensional bulk materials, integrated-over-angles spectroscopy yields a value of α varying from 0.9 to 1.2 [56–59].

The metallic 2 × 1 ⇔ semiconducting c(4 × 2) reversible phase transition on the β-SiC(100) surface at about 400 °C can be interpreted as a Peierls transition. Indeed, let the dimer chains exhibit one-dimensional properties and manifest their metallicity with period 1 along a chain (at $T > 400$ °C). Then, it is possible that, as the temperature lowers in the vicinity of 400 °C, electron–phonon interaction leads to Peierls instability, i.e., near the Fermi level there opens an energy gap related to the doubling of the lattice period and the emergence of charge-density waves, with the surface becoming semiconducting, as a result. Here the interaction between neighboring but distant chains becomes evident. This interaction manifests itself in the emergence of a c(4 × 2) reconstruction characteristic of the surface as a whole, i.e., the appearance of correlation in the direction perpendicular to the chains. The possibility of a phase transition emerges due to the finite interaction between neighboring chains, an interaction that extinguishes the strong fluctuations characteristic of ideal one-dimensional systems. If this effect were not present, the strong fluctuations would prevent the phase transition from occurring and would not let the energy of the system decrease because of a gap appearing near E_F.

To better understand the nature of this phase transition, Enriquez et al. [53] also conducted a photoemission study of the core level Si_{2p} of the β-SiC(100) surface for both reconstructions, the semiconducting c(4 × 2) reconstruction and the metallic 2 × 1 reconstruction. As shown earlier, for the semiconducting c(4 × 2) reconstruction the spectrum was decomposed into five components, two of which, S1 and S2, correspond to emission from dimers located above and below a certain median level. The two surface components are separated by 0.9 eV on the energy scale, with the charge redistributed between them. This picture corresponds to a doubled periodicity along the chain. Due to the phase transition, both surface components substantially decrease their amplitudes and a new component between them emerges, S*. Enriquez et al. [53] assumed that this new component is the result of emission from dimers belonging to the 2 × 1 reconstruction, which are located in the same median level (between S1 and S2) and. hence, have a median energy. Here the period along the chain becomes equal to 1. Apparently, what we have here is a partial phase transition, since according to the decomposition process domains of both reconstructions, 2 × 1 (predominant) and c(4 × 2), must coexist. The possible large fluctuations related to the phase transition (see above) may explain the coexistence of both

phases and, at the same time, indirectly corroborate the one-dimensional nature of the β-SiC(100) surface.

4. Silicon-rich β-SiC(100) surface

Increasing the amount of silicon on the β-SiC(100) c(4 × 2) surface above the stoichiometric composition leads to several other surface superstructures, with the 3 × 2 structure being the richest in silicon.

4.1 3 × 2 superstructure on the β-SiC(100) surface

The superstructure that is the richest in silicon on the β-SiC(100) surface, 3 × 2, is the easiest to access in experiments. This is probably why many more papers are devoted to this superstructure rather than to any other superstructure discovered on the surface in question. However, there are still no final irrevocable data (neither theoretical or experimental) on the exact amount of excess silicon corresponding to the 3 × 2 structure. Neither are there sufficient arguments in favor of this or that model. This section reviews the various viewpoints concerning the different models of this structure.

The silicon-terminated surface of the β-SiC(100) crystal of ideal stoichiometric composition consists of a single monolayer of silicon atoms. The different models can be broken down into groups according to the assumed excess amount of silicon on this surface. Three variants are discussed by both theoreticians and experimenters; the excess amount of silicon is 1/3, 2/3, and 1 monolayer. Table 4 lists the positive and negative factors characterizing the various models [41].

4.1.1 Models with 1/3 monolayer of excess silicon adsorbed on the surface. At present there are two models that assume that a 1/3 monolayer of excess silicon is present on the surface. These models are represented in Figs 10a and 10b.

The first model, known as SDRM (Single Dimer Row Model), was proposed by Hara et al. [12] and assumes that there is one adsorbed silicon dimer per 3 × 2 unit cell. These dimers are perpendicular to the dimers of the initial (prior to adsorption) c(4 × 2) reconstruction.

The second model, called ADRM (Alternate Dimer Row Model), was proposed by Yan et al. [60] on the basis of their *ab initio* calculations. It also assumes that there is one adsorbed silicon dimer per 3 × 2 unit cell. Here, it must be noted that the unit cells of these models are turned through 90° in relation to each other, so that, to be exact in surface reconstruction notation, one must bear in mind that the ADRM model describes a 2 × 3 reconstruction.

Both models also provide for the possibility that the silicon atoms of a filled monolayer reduce the number of dangling bonds and form dimers schematically depicted in Fig. 10 by dotted lines. Here, in the SDRM model there are two dimers per unit cell, while in the ADRM model there are three dimers per unit cell.

The STM topographs taken by Hara et al. [61] and Semond et al. [62] cannot be described by the SDRM model. Semond et al. [62] found that the dimers of adatoms in the 3 × 2 reconstruction are asymmetric and all slant in one direction. More than that, all the STM topographs show that the direction of the dimer bond is perpendicular to that of the dimer chains of the reconstruction (Fig. 10a), which contradicts the SDRM model. The calculations done by

Table 4. Generalization of the experimental and theoretical data on the β-SiC(100) 3 × 2 reconstruction and comparison of the models in question [41].

Model	Positive factors	Negative factors
SDRM	Coverage is comparable to the value found by Yoshinobu et al. Considered preferable to ADRM in calculations done by Pollmann's group.	Six dangling bonds in 3 × 2 reconstruction. Does not explain STM images. Considered less preferable than ADRM in calculations done by Yan et al. Gives no explanation of 3 × 2 → 3 × 1 transition stimulated by hydrogen
ADRM (Yan)	Coverage is comparable to value found by Yoshinobu et al. Considered preferable to SDRM in calculations done by Yan et al. Considered preferable in calculations done by Galli's group Better than other models corresponds to STM images obtained through simulation and band-structure calculations done by this group. Considered preferable to DDRM in calculations done by Shevlin and Fisher	Four dangling bonds per unit cell of reconstruction. Corresponds to 2 × 3 reconstruction instead of 3 × 2 reconstruction. Gives no explanation of 3 × 2 → 3 × 1 transition stimulated by hydrogen. Considered less preferable than ADRM in calculations done by Pollmann's group.
DDRM (Hara)	Allowed Hara et al. to explain their decomposition of Si_{2p} spectra. The only model that explains 3 × 2 → 3 × 1 transition stimulated by hydrogen.	Four dangling bonds per unit cell of 3 × 2 reconstruction. Less stable model in calculations done by Pollmann's group. Gives a poor explanation of STM images. Yields a coverage value incomparable to that found by Yoshinobu et al. Poorly corresponds to simulated STM images and band structure calculated by Galli's group. Considered less preferable than ADRM in calculations done by Shevlin and Fisher
TAADM (Pollmann)	Only two dangling bonds per unit cell of 3 × 2 reconstruction. The most stable model in calculations done by Pollmann's group. Explains STM images. Yields results that agree with band-structure data. (Apparently, corresponds to coverage value obtained by Yoshinobu et al.)	Yields strange value of coverage. Gives no explanation of 3 × 2 → 3 × 1 transition stimulated by hydrogen. Calculations done by Pollmann's group for 3 × 2 reconstruction are the same ones that corroborate MRAD for superstructure c(4 × 2) (or the MRAD model is invalid).

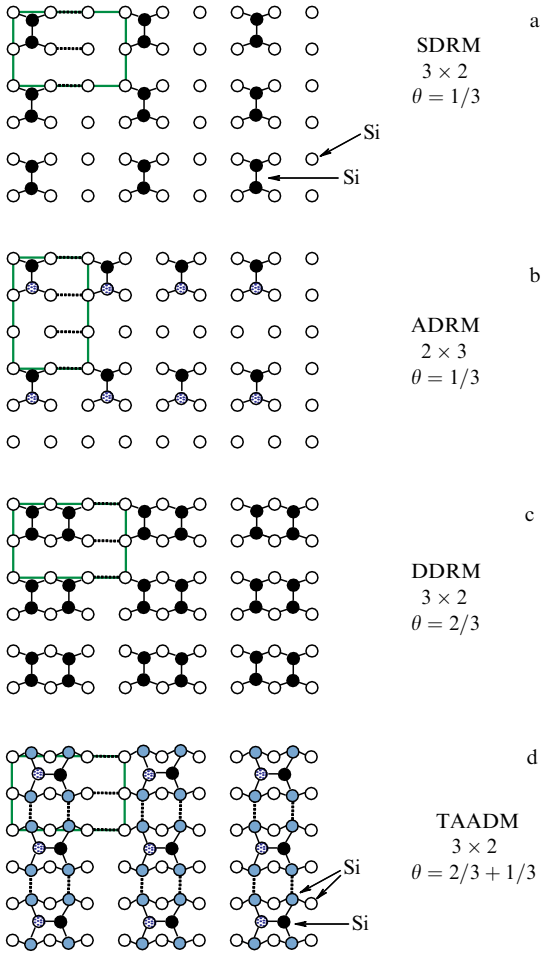

Figure 10. Models proposed for the β-SiC(100) 3 × 2 superstructure. θ denotes the excess silicon content in fractions of monolayer on the surface of the silicon plane. All the atoms depicted in this figure are silicon (in accordance with Ref. [41]).

Yan et al. [60] also show that this model has more drawbacks than the ADRM model. Still, in their later calculations, Pollmann and coworkers preferred the SDRM model (see Ref. [63]). However, they also found that both models are less stable than the model in which a larger number of excess silicon atoms cover the surface. To be just, we note that in their calculations Pollmann's group used 16 points of the Brillouin zone (see Ref. [63]), while Yan et al. [60] used only one point, which, naturally, reduced the reliability of the calculations done by the second group. The calculations of Pollmann's group (see Ref. [63]) showed that although the SDRM model is preferable to the ADRM model, still it gives no explanation of the simulation of STM images and the known experimental band-structure data [64, 65]. Thus, the SDRM model does not correspond to reality.

The ADRM model provides a good description of STM images and their simulation, but it does not correspond to reality either, since it contradicts the results obtained by using the LEED method. These results show that the direction of tripling of the 3 × 2 reconstruction coincides with the direction of doubling of the 2 × 1 reconstruction, in contradiction to the ADRM model, which describes the 2 × 3 model.

There are additional arguments that speak against both models (SDRM and ADRM). Dayan et al. [9] and later Hara and coworkers (see Ref. [66]) found that adsorption of atomic hydrogen initiates a 3 × 2 → 3 × 1 transition. At the same time, according to the ADRM model, even when dimer bonds are ruptured and the dangling bonds are saturated, the 2 × 3 reconstruction must retain its periodicity, i.e., remain a 2 × 3 reconstruction. Incidentally, that is also true of the 3 × 2 reconstruction in the SDRM model.

The picture of investigations of the 3 × 2 reconstruction that assume that there is a 1/3 monolayer of excess silicon atoms would be incomplete if we did not discuss the research of two other groups of scientists.

Galli's group (see Ref. [67]) did *ab initio* molecular dynamics calculations that led to the conclusion that the reconstruction corresponding to the ADRM model is more stable than the other two reconstructions (one of these has a 2/3 monolayer of excess silicon atoms). The simulation of STM images conducted by this group also shows a preference for the ADRM model rather than the SDRM model or the model that assumes there is a 2/3 monolayer of excess silicon atoms.

Recently Shevlin and Fisher [68] conducted *ab initio* calculations of the 3 × 2 reconstruction. They also compared the ADRM model with the model that assumes that there is a 2/3 monolayer of excess silicon atoms. Here, the SDRM model was entirely excluded. It was found that the ADRM model is more stable and corresponds better to the experimental band-structure measurements.

In conclusion of the discussion of this topic, we note that both models assume that the bonds of the dimers formed by the adatoms (ad-dimers) are perpendicular to the dimer bond of the 2 × 1 superstructure. Galli and coworkers (see Ref. [45]) calculated the possibility of an arrangement of the dimers in which the ad-dimer bond is perpendicular to the dimer bond in the 2 × 1 reconstruction. It was found that this situation is less preferable than the classical situation, where the dimers are mutually turned by 90°.

4.1.2 Model based on the adsorption of a 2/3 monolayer of excess silicon. A model with a 2/3 monolayer of excess silicon atoms was proposed by Dayan [9] and later developed by Kaplan [26] and Hara et al. [61]. This model, known as DDRM (Double Dimer Row Model) has two ad-dimers per unit cell of the 3 × 2 reconstruction (Fig. 10c). There are five different ways in which these two ad-dimers can be arranged in the unit cell. Hara et al. [61] proposed a model consisting of symmetric dimers (Fig. 10c). In the other four possible ways of arranging the dimers, the dimers are assumed asymmetric [63]

Hara et al. [61] state that their model explains the STM images taken by Semond et al. [62]. They assume that each spot in an STM topograph originates from a group of four excess atoms, i.e., actually, from two dimers. An image in the empty-states mode reflects the possibility of alternation of symmetric dimers arranged at different distances from the surface. The same group of researchers did a decomposition of the Si_{2p} level of the 3 × 2 reconstruction [38] into four components: one bulk component and three surface components. The surface component intensity ratio proved to be 2:1:1. It is assumed that the first component originates from four excess atoms, the second component from four atoms that are below the monolayer (each of which has a bond with one excess atom), and the third from two atoms that are below the monolayer (each of which has two bonds with excess atoms).

The DDRM model was corroborated by the molecular-dynamics calculations done by Kitabatake and Greene [69]. On the other hand, the calculations of Galli's group (see Ref. [67]) do not exclude the possibility that such a model can exist from the energy viewpoint, since its total energy only slightly exceeds that of the ADRM model. However, the STM images and the calculated band structure in DDRM do not correspond to the current experimental data. More than that, Galli's group (see Ref. [67]) showed that a DDRM-type model must have asymmetric dimers, which contradicts the assumptions made by Hara et al. [61] and Kitabatake and Greene [69].

In their recent *ab initio* calculations, Pollmann's group (see Ref. [63]) examined a model with a symmetric arrangement of two ad-dimers and found that this configuration is less stable in comparison to the other four configurations, in which the dimers are assumed asymmetric. More than that, the model proved to be less stable than the above two models with a 1/3 monolayer of excess silicon atoms. Band-structure calculations for the model with a symmetric arrangement of two ad-dimers have shown that HOMO (Highest Occupied Molecular Orbital) has a much larger dispersion in the $\Gamma-J$ direction compared to the dispersion measured in experiments by Lübbe et al. [64] and Hara's group (see Ref. [65]). More than that, the simulation of STM images done in the empty-states mode shows that for the 3×2 reconstruction in the DDRM model there must be four spots in the image, which also contradicts the experimental data. Thus, all the data in the literature make it possible to state that the DDRM model with a 2/3 monolayer of excess silicon atoms does not correspond to reality.

4.1.3 Model with a single excess silicon monolayer. Several years ago, Pollmann and coworkers (see Ref. [63]) proposed for the first time that the excess silicon concentration in the 3×2 reconstruction exceeds a 2/3 monolayer and is really a whole monolayer. They based their reasoning on the DDRM model with a 2/3 monolayer of excess silicon atoms. Then they assumed that there is a third 1/3 monolayer of silicon atop the second layer, with the new layer consisting of asymmetric dimers. They called this model TAADM (Two Adlayer Asymmetric Dimer Model). As the dotted lines in Fig. 10d show, the atoms of the second layer also form bonds, with the result that only two dangling bonds remain in a unit cell.

The authors of this model believe that TAADM provides a satisfactory explanation of all the current experimental data. First, they showed that the band structure calculated on the basis of this model is in good agreement with the results of current measurements [64, 65].

This means that the filled surface states have no dispersion in the $\Gamma-J$ direction (the direction of period tripling) and exhibit a dispersion of 0.37 eV in the $\Gamma-J'$ direction. Such behavior can be explained by the large distance between the first-layer dimers in the $\Gamma-J$ direction ($3 \times a_0$). In the $\Gamma-J'$ direction, the dimers can interact via the second-layer atoms. Next, the researchers show that the simulation of STM images based on their model provides a perfect explanation for the experimental data of Semond et al. [62]. This is reasonable, since, according to Semond et al. [62], a correct model must presuppose the existence of asymmetric dimers whose bonds are parallel to the direction of period tripling and perpendicular to the direction of the dimer chain. Actually, this is what the TAADM model assumes from the start.

Pollmann's group (see Ref. [63]) attempted, within their model, to explain the experimental result that Yoshinobu et al. [33] attained through the use of the RHEED (Reflection High Energy Electron Diffraction) method. Yoshinobu et al. [33] found that for the $c(2 \times 2)$ reconstruction, which is characteristic of a surface with a single carbon monolayer, to transform into the 3×2 reconstruction, the number of silicon atoms adsorbed by the carbon surface must be 1.36 times greater than that needed for the transformation to the 2×1 reconstruction. Actually, both ADRM and SDRM, which assume that there is a 1/3 monolayer of excess silicon on the surface, perfectly predict the same result. To bring their TAADM model into accord with the results of Yoshinobu et al. [33], Pollmann's group (see Ref. [63]) proposed a new model for the $c(4 \times 2)$ construction, which contains an additional 1/2 monolayer of silicon (the overall content of silicon atoms is 1.5 monolayers) [32]. In this case, according to Yoshinobu et al. [33], for the 3×2 construction the overall content of silicon atoms will be $1.5 \times 1.36 = 2.06$, which agrees quite well with the TAADM model (2 monolayers).

It must noted here that the calculations of Pollmann's group (see Ref. [63]) for the 3×2 construction are based on calculations for the MRAD model of the $c(4 \times 2)$ structure. However, below we will show that the MRAD model contradicts the experimental data very seriously. Hence, one must deal with the TAADM model with caution, too.

Finally, we note that there is no way in which the TAADM model can explain the $3 \times 2 \rightarrow 3 \times 1$ transition stimulated by adsorption of atomic hydrogen if, of course, we do not assume here that the coverage by excess silicon atoms decreases due to formation of Si_xH_y molecules leaving the surface. However, such a decrease in silicon concentration has never been recorded in experiments.

Table 4 presents a lucid generalization of the current experimental and theoretical data on the 3×2 reconstruction of the β-SiC(100) surface and a comparison of the models discussed above [41].

4.2 $m \times 2$ superstructure with $m = 2n+1$

As shown earlier, the 3×2 reconstruction of the β-SiC(100) surface is a structure with the largest number of excess silicon atoms on the (100) surface (i.e., largest compared to the stoichiometric composition). An ideal surface of a crystal of stoichiometric composition that is terminated by a single atomic silicon plane has the $c(4 \times 2)$ structure. If via desorption at $T = 1150\,^{\circ}C$ the number of excess silicon atoms is reduced, one can observe a transition from β-SiC(100) 3×2 to the $m \times 2$ superstructure, where m cannot be an even number, i.e., $m = (2n + 1)$: 5×2 or 7×2 [45, 67, 68]. It is assumed that the next superstructures are 9×2, 11×2, etc., but so far these reconstructions have not been observed in experiments. Note that the 3×2 structure also belongs to this group of surface superstructures ($n = 1$). More than that, we note that while for the 3×2 superstructure the excess of silicon above the stoichiometric composition amounts to a 1/3 monolayer, the excess of silicon for the structures discussed in this section (including 3×2) is determined by the quantity $\theta = 1/(2n + 1)$.

As in the case of the 3×2 superstructure, several models that explain these structures have been proposed. The various models are grouped in Fig. 11 using the 5×2 superstructure as an example. The SDRM and DDRM models are easily adapted to this case if the concentration of excess silicon is reduced from a 1/3 to a 1/5 monolayer and from a 2/3 to a 2/5

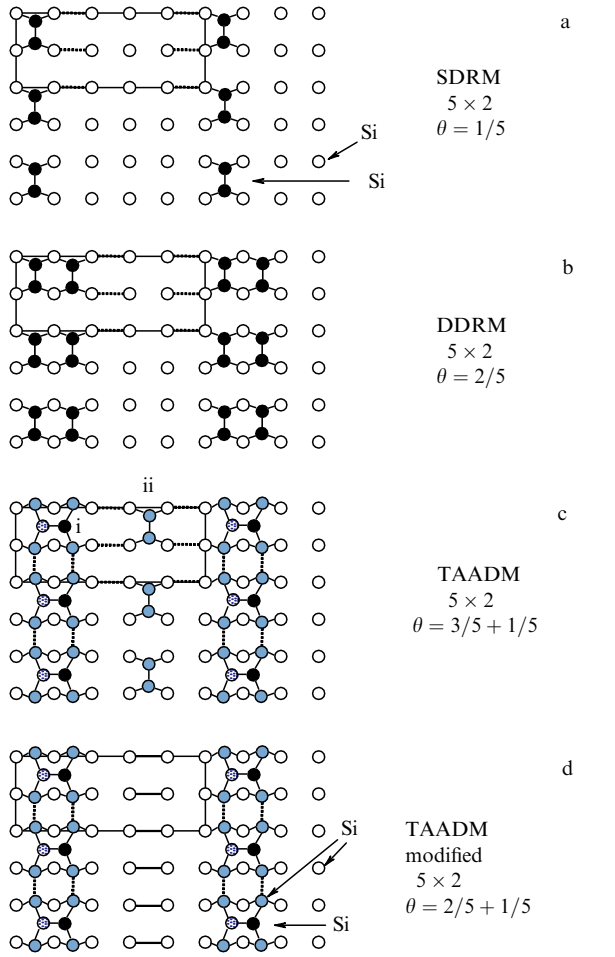

Figure 11. Models proposed for the β-SiC(100) 5 × 2 superstructure. θ denotes the excess silicon content in fractions of a monolayer on the surface of the silicon plane. All the atoms depicted in this figure are silicons (in accordance with Ref. [41]).

monolayer, respectively. As for the TAADM model, Pollmann and coworkers (see Ref. [44]) suggested placing between two standard dimer lines (denoted by i in Fig. 11) an additional dimer line with its bonds turned by 90° in relation to the bonds in the dimers belonging to the main lines (such an additional dimer line is denoted by ii in Fig. 11). These additional dimers belong to the lowest, completely filled, plane of silicon atoms [44]. The arguments for and against the concrete model of the 3 × 2 superstructure discussed above hold for the corresponding models of the 5 × 2 superstructure. Here, we note only that the number of dangling bonds for these three models of the 5 × 2 superstructure is 10, 8, and 4, respectively.

4.3 8 × 2 superstructure on the β-SiC(100) surface

Above, we have seen that the $m \times 2$ superstructure (with $m = (2n + 1)$: i.e., 3 × 2, 5 × 2, 7 × 2, etc.) on the surface β-SiC(100) of an ideal crystal terminated by an atomic silicon plane is the result of ordering of dimer rows. These dimer rows are formed by silicon atoms in excess of the stoichiometric composition, and until recently only reconstructions with odd values of m were discussed. Only in 1998 did Douillard et al. [70] show that the parameter m in the $m \times 2$ superstructures may be even.

The researchers deposited an excess amount of silicon onto an ideal β-SiC(100) surface. As a rule, short-duration annealing at $T \approx 1150$ °C lowers the concentration of excess (above stoichiometric composition) silicon and, as a consequence, leads to a sequence of structures: 3 × 2, 5 × 2, 7 × 2, etc. However, Douillard et al. [70] applied the LEED method and discovered that when the annealing time at 1150 °C is between the times necessary for the 3×2 and 5×2 structures to appear, a new superstructure forms, 8×2, which, due to its unusual position in the structure series, does not obey the rule $\theta = 1/(2n + 1)$.

This discrepancy was resolved by STM. Figure 12 depicts topographs of a 100 × 100 Å area of the surface with such a structure for filled (Fig. 12a) and empty (Fig. 12b) states. Clearly, the structure represents a self-ordering periodic sequence of pairs of dimer rows.

The distance $d_1 = 9 \pm 1$ Å (Fig. 12c) is the distance between neighboring dimer rows of the 3 × 2 superstructure, and $d_2 = 25 \pm 1$ Å is eight times the period of the substrate, which corresponds to an 8 × 2 superstructure and agrees with the LEED pattern. The distance between the closest rows belonging to neighboring pairs is 16 ± 1 Å, which is the distance between the neighboring dimer rows of the 5 × 2 superstructure. Thus, the 8 × 2 structure can be considered as being a sequence of pair dimer rows with long-range order or an alternate sequence of the smallest elements of the 3 × 2 and 5 × 2 superstructures: $3a + 5a = 8a$, where a is the substrate period. An elementary calculation shows that while the 3 × 2 superstructure contains a 1/3 monolayer of excess silicon, for the 8 × 2 superstructure the excess silicon concentration is $\theta = 1/4$.

Thus, as the excess silicon content is reduced to below the stoichiometric on the β-SiC(100) surface, the following sequence of superstructures and compositions proceeds: 3×2 ($\theta = 1/3$), 8×2 ($\theta = 1/4$), 5 × 2 ($\theta = 1/5$), 7×2 ($\theta = 1/7$), etc. (the compositions are given on the assumption that the 3 × 2 superstructure has an excess silicon content of $\theta = 1/3$).

The properties of these superstructures — the linearity of the chains and the fact that the chains are one-dimensional and straight — makes them potential objects for using in nanoelectronics, especially when the density of atomic lines in the direction perpendicular to the chain has to be controlled. Hence, we believe it is important to study the thermal stability of such structures. The results of research in this field are discussed in the next section.

4.4 One-dimensional self-organizing chains of silicon dimers on the surface of cubic silicon carbide. Thermal stability and destruction mechanisms

Here, we will show that, in the process of phase transition from the silicon-rich β-SiC(100) 3 × 2 reconstruction to the β-SiC(100) c(4 × 2) reconstruction (also formed by silicon atoms but of stoichiometric composition), straight self-organizing lines consisting of chains of dimers of silicon atoms are formed. The structures that emerge prove to be stable up to 900 °C.

For the β-SiC(100) 3 × 2 reconstruction, which has the maximum of excess silicon, to transform into the stoichiometric β-SiC(100) c(4 × 2) reconstruction, the sample's temperature must be maintained for a certain time at $T \approx 1150$ °C to remove the excess of silicon. When the annealing times are short, superstructures are formed that consist of the one-dimensional chains mentioned earlier: 8 × 2 ($\theta = 1/4$), 5 × 2 ($\theta = 1/5$), and 7 × 2 ($\theta = 1/7$); here

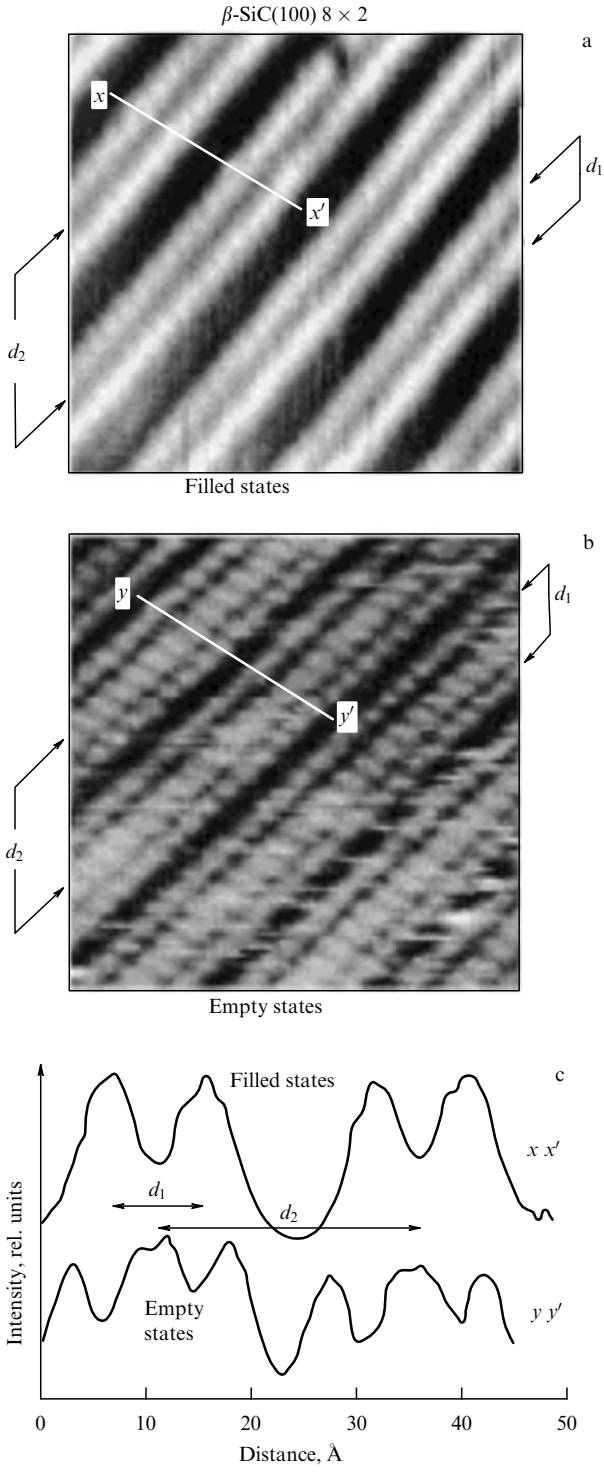

Figure 12. 100 × 100 Å STM topograph of the β-SiC(100) 8 × 2 superstructure taken in the following modes: (a) filled-states mode ($V = +3.55$ V and $I = 0.3$ nA), and (b) empty-states mode ($V = -2.75$ V and $I = 0.3$ nA). (c) The topograph profiles measured across dimer rows; d_1 and d_2 are, respectively, the distances between rows in a pair and between the nearest pairs [70].

the values of θ are based on the assumption that $\theta = 1/3$ for the initial 3 × 2 superstructure [44]. More than that, Soukiassian's group found that, as a result of a transition from the 3 × 2 superstructure to the stoichiometric reconstruction c(4 × 2), dimer chains separated by rather large distances and even individual dimer lines may emerge [28, 43, 71, 72]. Dimer chains are one-dimensional, straight, and continuous formations (within a given terrace) whose density in the direction perpendicular to the chain line can be controlled. Figure 13 depicts a sequence of STM 800 × 800 Å topographs of the β-SiC(100) surface at 300 K taken after annealings of different duration at 1150 °C.

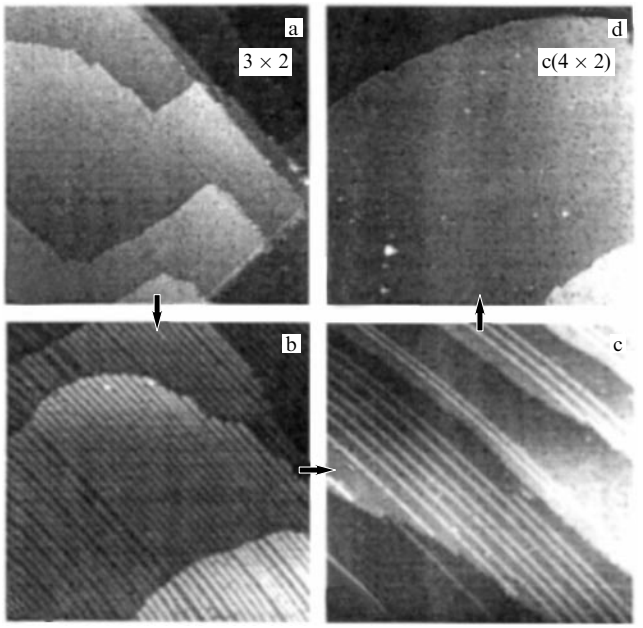

Figure 13. 800 × 800 Å STM topographs of the β-SiC(100) surfaces: (a) the β-SiC(100) 3 × 2 reconstruction; (b) high-density dimer lines of Si atoms; (c) the same as in (b) but with lower line density [a c(4 × 2) reconstruction can be seen between the lines]; and (d) a c(4 × 2) reconstruction of the surface ($V = +3.0$ V and $I = 0.2$ nA) [72].

These nanoobjects, which are lines of silicon dimer chains, self-organize on the β-SiC(100) surface and possess unique properties, which place them quite apart from nanoobjects fabricated earlier by, say, adsorption of metals on silicon surfaces [28, 48]. These new nanoobjects possess the following properties:

- they consist of Si – Si dimers;
- they are very long (their length is limited only by the size of terraces on the surface);
- they can be fabricated as a result of single-stage treatment, namely, annealing at a certain high temperature;
- the number of them and the distance between them can be determined beforehand by selecting the duration and temperature of annealing; in this way, one can fabricate (depending on what one desires) a broad spectrum of nanostructures: from a superlattice with a minimum period of 6.16 Å to a single isolated atomic line.
- they are formed on the surface of a wide-gap semiconductor, which means that they are interesting objects for studying transport properties, i.e., they are much more stable than other known nano- and sub-nanostructures [28, 48].

As is known, β-SiC is a high-temperature semiconductor with a set of especially unique properties. Bearing in mind that, in many cases, in the manufacture of devices it is necessary to employ nanotechnologies, there is a need to study the dynamics of the transformation of the discovered nanoobjects (silicon atomic lines) caused by the changing temperature. Until recently there were no such studies of the

stability of nano-objects at high temperatures and there were practically no data on the behavior of such objects at extreme temperatures.

In order to inspect the thermal stability of the new one-dimensional chains, STM studies were conducted that enabled the researchers to investigate a surface at temperatures as high as 950 °C [73]. The researchers found that, irrespective of the history of the object, lines consisting of dimers of Si atoms remain stable on heating up to $T \leqslant 900\,^{\circ}\mathrm{C}$ but begin to disintegrate at $T \sim 900\,^{\circ}\mathrm{C}$ [73]. (This is, probably, the highest temperature at which STM studies have ever been conducted.) They established that the one-dimensional chains are destroyed either by removing individual dimers (the individual mechanism) or by shifting whole atomic lines in the direction perpendicular to the line (collective mechanism).

The experiment was conducted using an Omicron VT-STM scanning tunneling microscope, which operates in a temperature range from $-230\,^{\circ}\mathrm{C}$ to $+900\,^{\circ}\mathrm{C}$. The pressure in the spectrometer was maintained at 10^{-11} Torr up to sample temperatures of roughly 925 °C. At high temperatures the time required for stabilizing the temperature drifts did not exceed 60 min.

Let us examine the effect of temperature on the lines of Si atoms. Figure 14 depicts 300 × 300 Å STM topographs of such lines taken at room temperature (left topograph) and at 1000 K (right topograph). The topograph taken at room temperature shows silicon lines consisting of individual dimers, which is in full agreement with the results of earlier studies [71]. As the temperature is raised to 1000 K, not one of the lines acquires discontinuities. More than that, as at room temperature, the distance between the silicon lines remains unchanged, the lines are parallel and form a regular pattern of the 7 × 2 structure.

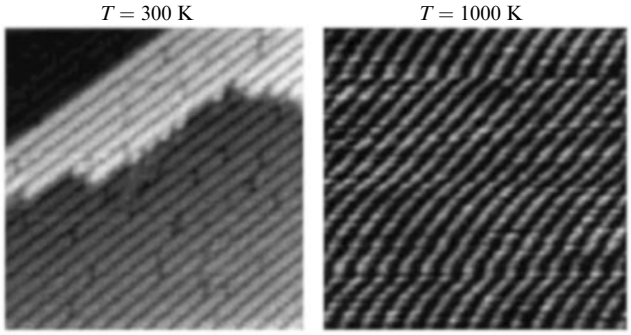

Figure 14. 300 × 300 Å STM topographs of Si atomic lines on the β-SiC(100) surface taken at 300 K and 100 K [73].

At 1100 K, transformation of the self-organizing nanostructure begins. We study the evolution of these changes by selecting a section of the topograph and follow its evolution in time at the same temperature, 1100 K. Figure 15 depicts a sequence of eight 300 × 300 Å STM topographs each taken at 1100 K, with the overall measurement times (from the first to the eighth topograph, Figs 15a–15h) amounting to 25 min. Two defects on the surface, denoted by $D1$ and $D2$, are used as markers for tracking one and the same section of the surface. In all eight topographs the positions of the markers $D1$ and $D2$ remained unchanged, as, incidentally, the density of all lines in the specified section. The line XX' is especially interesting for observation. It lies between the markers $D1$

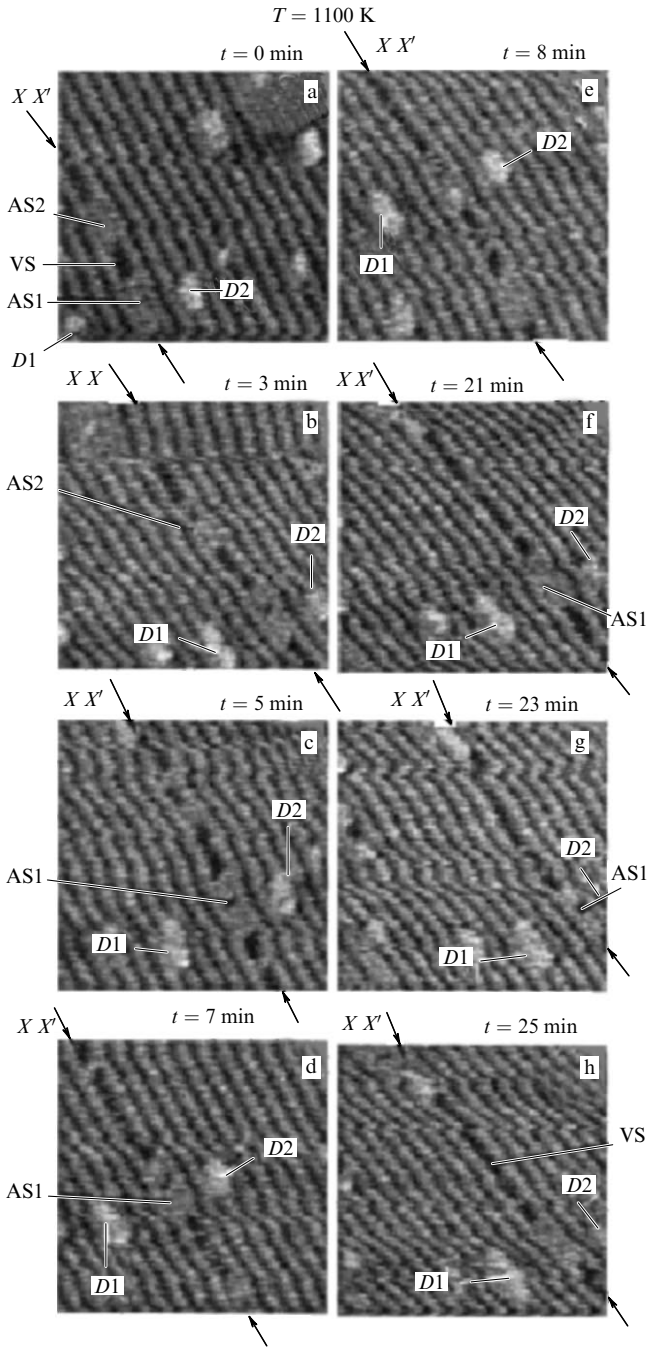

Figure 15. Sequence of eight (a–h) 300 × 300 Å STM topographs of Si dimer lines at 1100 K (0–25 min) demonstrating destruction on the XX' line of the dimer segments AS1 and AS2, which transform into the vacant segment VS. The defects $D1$ and $D2$ serve as markers for tracking one and the same section of the surface [73].

and $D2$ and has two segments, denoted by AS1 (ten dimers) and AS2 (eight dimers), separated by a vacancy segment VS (approximately five absent dimers) (Fig. 15a). The distance between dimers along an atomic line is 6.16 Å.

After 3 min, as Fig. 15b shows, AS1 and AS2 lose one and two dimers, respectively, while VS becomes longer (seven absent dimers). Thus, AS2 moves away from AS1, which does not change its position. Two minutes later (Fig. 15c), AS1 has not changed, but AS2 has lost more dimers and VS has increased its length by one more absent dimer. After 7 min from the beginning of observation, AS2 has only one dimer

left, while the length of VS reaches a value equal to 14 absent dimers. This means that the remaining segment AS2 is still moving away from AS1 (Fig. 15d). In the interval from 8 min to 25 min, the last dimer belonging to AS2 disappears, with VS increasing its length to 25 absent dimers. Thus, the evolution of the selected section of the image demonstrated the mechanism of destruction of a dimer line consisting of silicon atoms.

To determine the temperature limit of stability of atomic lines, the effect of two higher temperatures, 1200 K and 1225 K, was studied. At 1200 K the continuous atomic lines in the beginning of annealing exhibit fairly regular alternation. However, further annealing at this temperature leads to substantial disturbances: the density of these lines drops considerably and begins to vary from one section of the surface to another; more than that, some sections show a total absence of lines. The change in the distance between the various sections of neighboring lines suggests that the lines move laterally, i.e., in the direction perpendicular to the lines. For silicon dimer chains, the temperature 1200 K is probably the limit. For a final verification of this assumption, the temperature in tests was increased to 1225 K. Indeed, even such a small increase in temperature (only by 25 K) led to dramatic changes. Obviously, the operational limit of the device had been reached.

Thus, the described STM measurements suggest that at high temperatures there are two mechanisms of behavior of silicon atomic lines, individual and collective. The individual mechanism amounts to removal of the individual atoms and/or dimers one at a time. The collective mechanism amounts to collective lateral motion of the silicon line as a whole.

5. Carbon-terminated β-SiC(100) surface of stoichiometric composition formed by a single monatomic carbon layer

5.1 c(2 × 2) reconstruction of carbon-terminated β-SiC(100) surface of stoichiometric composition

As shown at the beginning of the review, the β-SiC crystal may be considered as consisting of Si and C planes of monatomic thickness alternating in the direction $\langle 100 \rangle$. Hence, depending on which plane is the outer one, one can have a (100) surface consisting either entirely of Si atoms or entirely of C atoms. In the previous sections, we discussed the surface consisting of silicon atoms. Now, we tern to the second case, where the surface monatomic layer consists entirely of carbon atoms.

In their first studies, Dayan [9], Bellina and Zeller [74], and Kaplan [26], who used a carbon-terminated β-SiC(100) surface, found that the surface is reconstructed c(2 × 2). Later, in several papers it was reported that this reconstruction corresponds to 1 monolayer of carbon [12, 33, 75 – 78].

The most probable structure of the crystal surface that is a plane of atoms with the coordination number equaling four, as is the case with C(100), Si(100), or Ge(100), is a structure formed by 1 × 2 dimers (Fig. 16a). Here, we have written 1 × 2 to emphasize the fact that the dimer bonds are turned by 90° relative to the dimers on the same surface but with silicon atoms instead of carbon atoms. Two models were proposed to explain the formation of the c(2 × 2) reconstruction on the surface.

The first model presupposes a structure formed by classical dimers resembling dimers of the 2 × 1 reconstruction of silicon and diamond and aligned not along straight lines but with a shift, so that they form a c(2 × 2) reconstruction. This model is known as the shifted dimer model (Fig. 16b). The carbon atoms have an electron configuration of the hybridized type, sp^3, and a single dangling bond per atom. Here, the plane of silicon atoms that is below the terminating carbon plane has completely saturated bonds. This model was first proposed in 1990 by Hara et al. [12] and further developed in 1991 by Bermudez and Kaplan [78] on the basis of data on Auger-electron spectroscopy (AES), LEED, electron energy loss spectroscopy (EELS), and stimulated H^+ desorption [78]. Bermudez and Kaplan also showed that the length of the dimer bond is 1.54 Å.

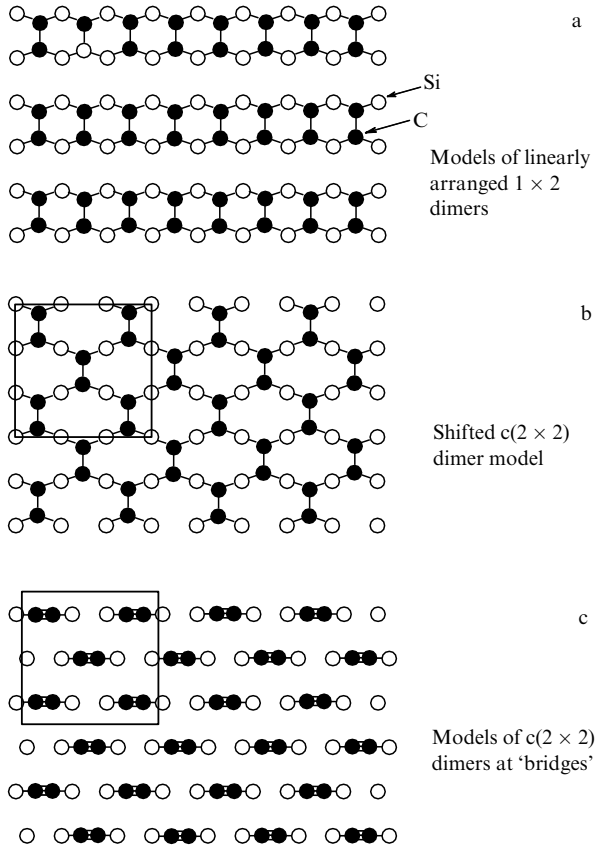

Figure 16. Structure models proposed for the β-SiC(100) c(2 × 2) superstructure formed by a single carbon atomic plane (according to Ref. [41]).

The second model capable of explaining the c(2 × 2) reconstruction is very unusual. It was proposed in 1991 by Powers et al. [79], who employed automated tensor (dynamical) low-energy electron diffraction to analyze the reconstruction. This model also uses dimers, but each carbon atom has the electron configuration sp^2 and has only one bond with a silicon atom (Fig. 16c). It is called the model of dimers at 'bridges'. The two atoms belonging to a dimer are connected by one bond of the σ type and one π bond, with one dangling bond remaining at each carbon atom. The dimer length in this model is 1.31 Å due to the strong double bond between carbon atoms.

There are two different methods of preparing the c(2 × 2) surface:

(1) desorption of surface silicon from the c(4 × 2) surface by high-temperature annealing;

(2) deposition on the c(4 × 2) surface of a monolayer of carbon obtained by decomposition of molecular ethylene.

According to Powers et al. [79], in the first method of preparing the structure, weak silicon dimer bonds are formed in the second atomic layer of the c(2 × 2) surface produced by silicon sublimation, while in the second method, dangling bonds remain on the silicon atoms during ethylene deposition.

In the same year (1991), Badziag [18] did calculations that corroborated the model of dimers at bridges. Here, the bond length was found to be 1.2 Å, which actually means the presence of a triple bond. Badziag [18] proposed that the hybridization of the electrons is of sp type, which is close to the model of Powers et al. [79], but means that the bond is stronger, since the two dangling bonds form a second π-bond. This model also assumes that the silicon atoms in the layer below the terminating carbons layer form dimers.

The argument over which of the models is more realistic was resolved in 1996. Long, Bermudez, and Ramaker [80] used NEXSAFS and photoemission data and unambiguously showed that the true model is that of dimers at bridges. According to these researchers, the electron configuration is an intermediate one between sp^2 and sp, and is closer to the configuration with a triple bond. This means that the bridge formed by a carbon dimer is closer to the horizontal position than in the case of the electron configuration sp^2. Their data clearly show the direction of each bond and corroborate the fact of dimer formation in the layer below the terminating carbon layer.

In a later investigation, Yeom et al. [81] used experimental STM data, photoelectron diffraction (they measured the intensity of core-level spectra as a function of the exciting-photon energy), and angle-resolved spectroscopy to corroborate the model of carbon dimers with triple bonds (closer in nature to sp than to sp^2) at bridges.

The angle-resolved photoelectron-spectroscopy data made it possible to identify two surface (S1 and S6) and four resonance (from S2 to S5) states. Two of these, S1 and S2, which are near the Fermi level (∼2.2 eV and ∼3 eV at the Γ point), are σ bonds of carbon dimers (hybridized with dangling silicon bonds), which means that they contribute the most to the STM topographs taken in the filled-states mode. The two resonant states S3 and S4 are π bonds in the directions z and x (∼4.6 eV and ∼5.6 eV from the Γ point). These orientations were corroborated in measurements involving polarized radiation. Finally, the resonance state S5 and the surface state S6 (∼7.8 eV and ∼10.1 eV at the Γ point) were identified as the C–Si bonds of carbon dimers. Note that the surface states are in the forbidden band and do not overlap (in energy) with bulk states; this sets them apart from resonance (surface) bonds.

Yeom et al. [81] noted that the two π bonds of the c(2 × 2) superstructure have higher energies than the π bond of the C(100) and Si(100) surfaces. It is assumed that this explains the stability of the model, which is not minimized in the number of unsaturated (dangling) bonds. Finally, the researchers found that the length of the dimer bond is 1.22 Å, which corresponds to the triple bond of an acetylene molecule (pure sp hybridization).

Derycke [41] has pointed out that the experimental and theoretical agreement concerning the model of the carbon-terminated β-SiC(100) c(2 × 2) surface serves as an additional argument against the MRAD model of the c(4 × 2) surface reconstruction of the silicon-terminated surface. For instance, if we assume that MRAD is a correct model, this means, first of all, that the outer surface of the crystal has 1.5 monolayers of silicon instead of 1 monolayer. In this case, adsorption of ethylene at the surface cannot lead to the formation of a c(2 × 2) reconstruction with dimers at bridges. Although this argument has never been used against the MRAD model, it is the strongest one, since it is firmly corroborated by experimental data.

A large amount of theoretical work has also been done in this field. All semiempirical calculations [82–86], with the exception of Badziag's paper [18], corroborate the shifted dimer model. On the other hand, *ab initio* calculations [25, 87–91] support the model of dimers at bridges with a triple C–C bond.

It must also be said that all the theoretical calculations have established for a surface consisting of carbon that the difference between binding energies in the models considered is very small. Some researchers conclude that on the basis of their calculations [18, 88, 91] it is difficult to identify the most stable model. Others deduce that this small difference in energies between the various models may mean that several different structures coexist on the surface [18, 25, 88]. Recent STM studies conducted by Derycke et al. [92] corroborate this opinion. Figure 17 depicts STM topographs of the c(2 × 2) reconstruction taken from a 40 × 40 Å area in the filled-states mode (a) and in the empty-states mode (b).

Figure 17a clearly shows that the image consists of bright spots corresponding to c(2 × 2). The intensity profile recorded along the XX' line (below the STM topograph) reveals that the distance between neighboring spots is 5.75 Å, which is close to 6.16 Å, the value expected for c(2 × 2). Hence, the researchers identify each bright spot in the topograph with a carbon dimer.

The topograph of the same section of the surface but taken in the empty-states mode is depicted in Fig. 17b. Every spot in Fig. 17a corresponds to two spots in Fig. 17b, each smaller than the former. Here, we already have one carbon atom corresponding to a spot. More than that, the image also makes it possible to determine the direction of the dimer bond of the carbon atoms in relation to the substrate.

However, the most interesting fact is that the height at which the carbon atoms in a dimer are arranged is different in relation to the substrate. This is clearly evident from the height profile measured along the XX' line (the profile is below the STM topograph in Fig. 17b). This leads to a new important conclusion, namely, that all the carbon dimers of the c(2 × 2) reconstruction are asymmetric and slanted in the same direction. Here, obviously, there is also charge transfer from one carbon atom to the neighboring atom of the same dimer, which is quite common in classical dimers, as shown by the Si(100) c(4 × 2) surface. In this case, however, in contrast to silicon, we are dealing with dimers with a triple bond. More than that, no one of the numerous calculations, either semiempirical or *ab initio*, predicts that these dimers are asymmetric. Derycke et al. [92] believe that the stressed state of the surface characteristic of SiC crystals plays the key role in the redistribution of charge between the dimer atoms and results in the dimers being asymmetric.

5.2 Carbon dimer chains on the c(2 × 2) surface

5.2.1 Experimental observation of carbon chains on the c(2 × 2) surface. The possibility of dimer lines of silicon atoms forming on a silicon-terminated β-SiC(100) surface is a characteristic and promising property of this surface. It would be interesting

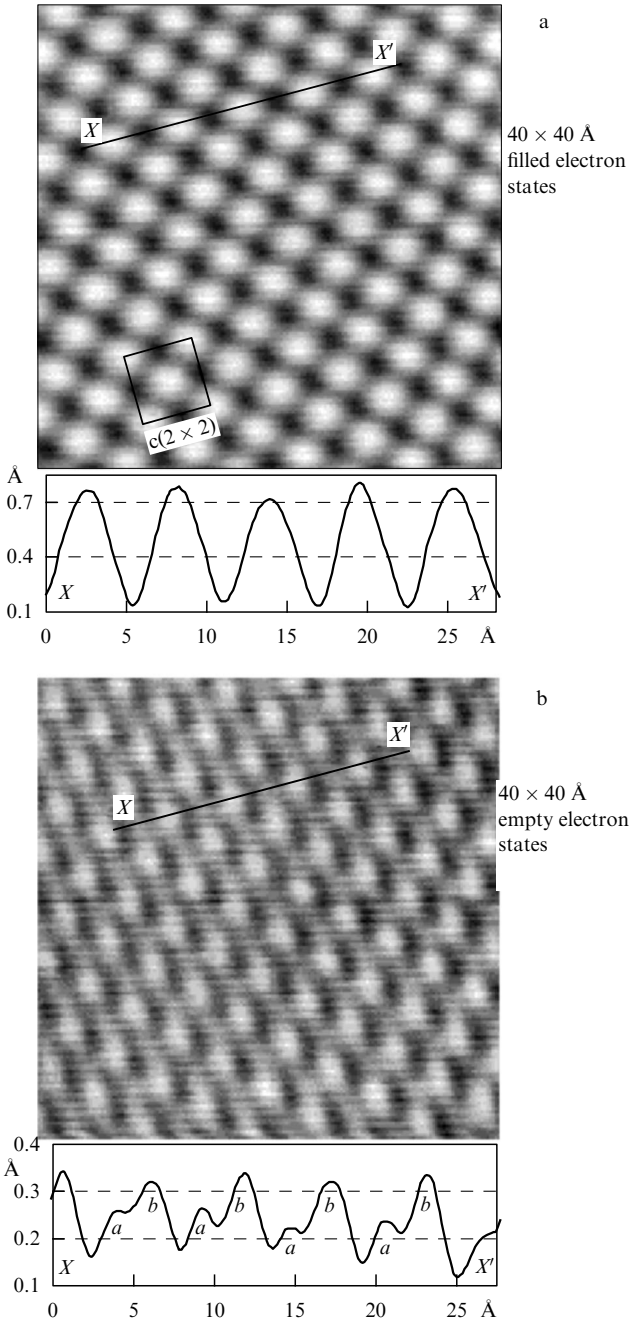

Figure 17. STM topographs of the c(2 × 2) surface [92]: (a) filled electron states ($V_t = -3$ V) and (b) empty electron states ($V_t = +3$ V) (in both cases $I_t = 200$ nA). The intensity profiles in the directions XX' are shown below the respective topograph.

to discover something similar for a carbon-terminated β-SiC(100) surface. Derycke et al. [93] studied this problem. As is known, the c(2 × 2) reconstruction is extremely stable up to $T \sim 1150\,^{\circ}$C, but at $T \sim 1250\,^{\circ}$C graphitization of the surface occurs due to excess concentration (compared to the stoichiometric composition) of carbon on the surface. In order to fabricate one-dimensional structures, Derycke at al. [93] annealed samples with the c(2 × 2) reconstruction at different temperatures and found that at $T \sim 1200\,^{\circ}$C (prior to graphitization) a new type of one-dimensional structure is formed. They also found that the larger part of the surface has the well-known structure of the c(2 × 2) reconstruction, while against this background one can observed bright chains with the following properties:

- all chains point in the same direction;
- chain length varies from several angstroms to several hundred angstroms;
- chains may begin and end at various points, including terrace edges;
- the distance between chains may be different, and formation of agglomerates may also be observed;
- some sections of chains may deviate from a straight line.

The above properties differ substantially from those of silicon dimer chains on the c(4 × 2) surface, on which, in particular, the chains are always straight.

Figure 18 depicts detailed STM topographs of c(2 × 2) [93] with the chains mentioned above. Figure 18a is the topograph taken in the empty-states mode. Clearly, each element of a chain corresponds to two bright spots forming a zigzag. The topograph in Fig. 18b is the image of the same section of the surface but taken in the filled-states mode. Two important differences from Fig. 18a are clearly visible:

(1) each dimer is represented by a single spot;

(2) all spots are positioned at the same height.

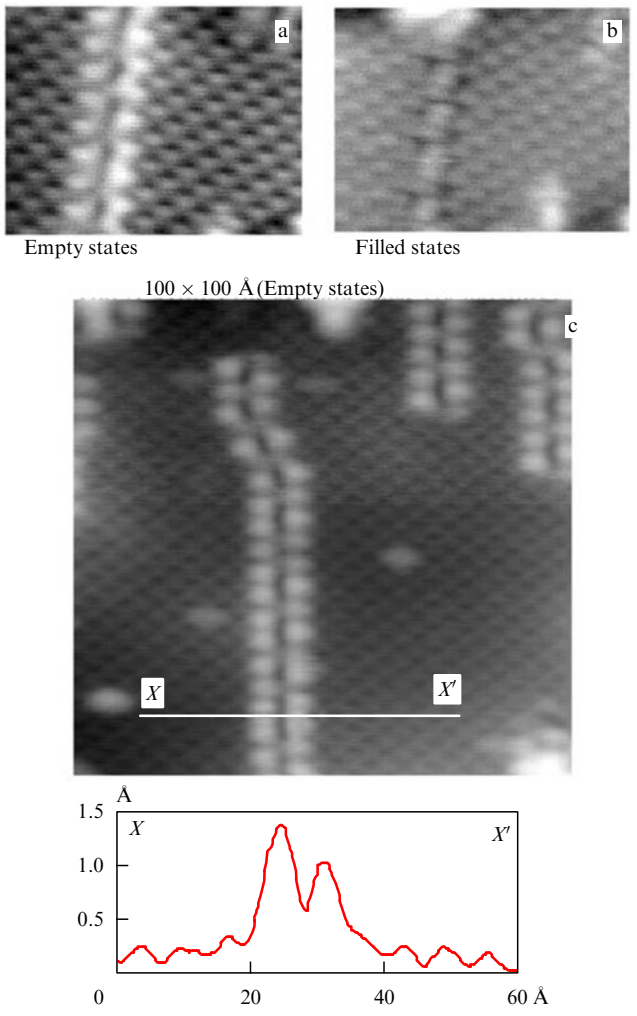

Figure 18. Detailed images of one-dimensional chains: (a) 50 × 65 Å (empty states), (b) 50 × 65 Å (filled states), and (c) 100 × 100 Å (empty states) and intensity profile in the direction XX'. In all three images, $V_t = \pm 3$ V and $I_t = 200$ nA [93].

Thus, Fig. 18b implies that the chains are in the same atomic plane as the atoms of c(2 × 2).

Figure 18c depicts the profile of the image height in the direction perpendicular to the chain direction. Clearly, empty states corresponding to the 1D structure are positioned ~1 Å above the states of the main surface. More than that, this profile suggests that the dimers are asymmetric, which results in the zigzag nature of the chain images.

To determine the stability of the chains, Derycke et al. [93] subjected the given structure to a series of annealings and found that the chain density increases, with the result that eventually the entire surface is covered by chains.

5.2.2 Models of chains on the c(2 × 2) surface. As a result of their studies of the structure of chains on the c(2 × 2) surface, Derycke et al. [93] proposed the following model. During annealing at high temperatures, some of the carbon dimers, which initially have an sp-type triple bond, acquire the classical sp^3 configuration. Such a transformation requires a turning of dimers through 90° and reorganizing the reverse Si–C bonds. Classical dimers organize into lines of different length. Here, each spot in the STM topograph taken in the filled-states mode corresponds to one dimer, while on the STM topograph taken in the empty-states mode, each spot corresponds to one atom. The alternating intensity of the spots is caused by the asymmetry of the dimers, which explains the zigzag shape of the chains.

In this model, the chain atoms belong to the same monatomic plane of carbon atoms as the atoms of the main c(2 × 2) reconstruction. This statement is an obvious corollary of the topographs of the structure taken in the filled-states mode (see above). In the empty-states mode, the chains in the image appear to be raised above the main atomic plane due to the presence of two dangling bonds, which are absent from the main c(2 × 2) reconstruction because of the formation of triple bonds in the dimers. The schematic of the model is shown in Fig. 19, where straight and bent chains of dimer lines are depicted against the general 'background' of the c(2 × 2) reconstruction.

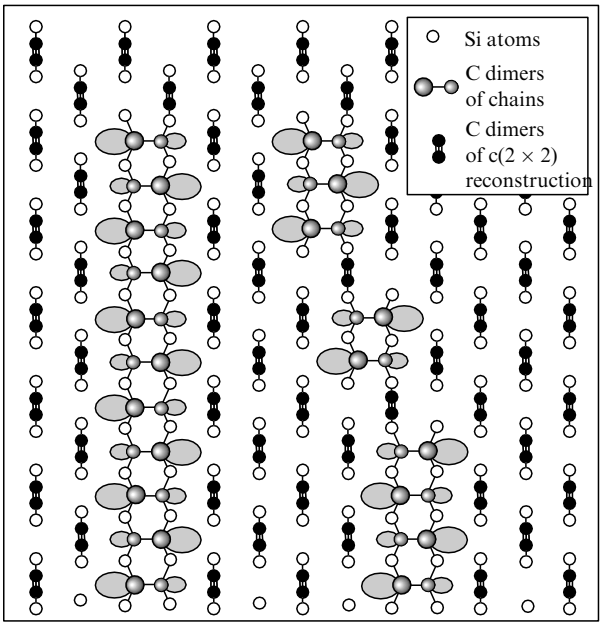

Figure 19. Structure model of the carbon surface (100) of silicon carbide containing one-dimensional straight and bent chains [93].

This model has been corroborated in various theoretical calculations done, for instance, by Yeom et al. [38], Kaplan and Bermudez [47], and Dyson and Smith [85]. However, the most interesting confirmation of the validity of the model has been established by Galli's group (see Ref. [94]). Using the state-of-the-art methods of calculating the possible structures on a carbon surface, these researchers arrived at the following conclusions:

- the difference in energy for the configurations of the c(2 × 2) reconstruction of the sp type and that formed by sp^3 dimers is small and amounts to about 65 meV per dimer. Here, in the absence of stresses, the c(2 × 2) reconstruction is the most stable one;
- the higher the density of sp^3-type dimers, the lower the energy required for their formation;
- calculations show that the presence of vacancies of sp dimers in the c(2 × 2) reconstruction lowers the barrier for the sp → sp^3 transition.

(Note that Derycke et al. [93] observed only a certain percentage of vacancies in the STM images of the c(2 × 2) reconstruction, which, according to the given calculations, should facilitate the observed chain formation.) A simulation of STM images done by Galli's group (see Ref. [94]) agree perfectly with the STM topographs of the c(2 × 2) reconstruction and one-dimensional chains taken in the experiments of Derycke et al. [93].

6. Conclusion

By the beginning of the 1990s, substantial advances in growing high-quality single crystals of silicon carbide had been made. This brought about an upsurge of interest of both experimenters and theoreticians in the β-SiC(100) surface. The reason for this was not only the need for new electronic devices that could operate at higher temperatures than those at which silicon-based devices operate. Another reason for this, especially interesting for theoreticians, was the fact that the silicon-terminated β-SiC(100) surface of stoichiometric composition has the same structure as the (100) surface of silicon crystals but that the atomic separation on the surface is 20% smaller. This is why in the period covered by the present review so many theoretical papers devoted to the 2 × 1 structure appeared. However, it has been found that at room temperature no such structure exists on a clean surface, and so these papers were practically ignored in this review.

Intensive investigations made it clear exactly what superstructures could form on clean surfaces and what properties these superstructures would have. Researchers have found that the main structure on the silicon-terminated surface of silicon carbide of stoichiometric composition is c(4 × 2) and that this structure exhibits semiconductor properties. They have established that the arrangement of the dimers of this structure differs dramatically from that of the dimers of a similar c(4 × 2) reconstruction of the (100) surface of silicon, which exists at reduced temperatures. However, we do not know of any theoretical studies of the electron band structure of the c(4 × 2) surface. It has been found that the 2 × 1 reconstruction exists at $T \geqslant 400\,^{\circ}C$ and is metallic, while in silicon this structure exists at room temperature and is semiconducting. The possibility of fabricating self-organizing one-dimensional straight chains of silicon-atom dimers on

the silicon-terminated β-SiC(100) surface is quite remarkable. Here, the chain length is determined solely by the terrace size, while the distance between the chains can be varied from six to hundreds of angstroms. There can even be one line on the entire terrace. The effect of oxygen, hydrogen, and alkali metals on the properties of the discovered superstructures is being studied, but this topic was not discussed in the present review.

Despite the obvious progress in understanding the structure and properties of a clean β-SiC(100) surface, much has been insufficiently studied or remains unknown. For instance, the 3×2 superstructure of the Si-rich surface is the most studied (according to a number of publications) and the easiest to prepare. However, there is still no agreement between different groups of scientists not only on what model this reconstruction corresponds to, but also on what number of excess silicon atoms this superstructure contains (1/3, 2/3, or 1 excess monolayer). The argument will probably be resolved only after this structure is studied by the X-ray diffraction method involving synchrotron radiation in the geometry of small angles between the primary beam and the surface under investigation (about 0.5°). We believe it is necessary to continue studies of the electronic properties of linear chains formed by silicon dimers and to investigate the possibility of using such chains in nanoelectronics. A lot has to be done in studies of the interaction of both submonolayer and multilayer metals and the different superstructures of the substrate, which would play an important role in the development of various electronic devices. Thus, it is obvious that there is much to be done before the structure of the β-SiC(100) surface is fully understood. Nevertheless, we believe that because of the remarkable properties of silicon carbide, which in many respects considerably exceed the similar properties of silicon, and because of the ever increasing efforts in studying the structure and properties of the surface of this material, in the years to come devices based on silicon carbide will occupy their rightful place in micro- and nanoelectronics.

Acknowledgments

I am grateful to Academician Yu A Osip'yan for numerous discussions, useful remarks, and unflagging interest in the work; to Prof. P Soukiassian, Dr. H Enriquez, and M D'Angelo (Commissariat a l'Energie Atomique, Saclay, France), Dr. V Derycke (IBM, USA), and Dr. F Amy (Bell Labs., USA) for interesting discussions on the topics covered in this review and for providing material for the figures; and especially to Prof. Yu M Tairov (Electrotechnical Institute, St. Petersburg, Russia) for kindly supplying the difficult-to-obtain samples.

This work was supported in part by the Russian Foundation for Basic Research (project No. 99-02-16157).

7. Appendix

References

1. Tairov Yu M *Mater. Sci. Eng. B* **29** 83 (1995)
2. *Silicon Carbide. A Review of Fundamental Questions and Applications to Current Device Technology* Vol. I & II (Eds W J Choyke, H Matsunami, G Pensl) (Berlin: Akademie Verlag, 1998)
3. Silicon Carbide Electronic Devices and Materials *Mater. Res. Soc. Bull.* **22** (1997)
4. Silicon Carbide Electronic Devices *IEEE Trans. Electron Dev.* **46** (Special Issue) (1999)

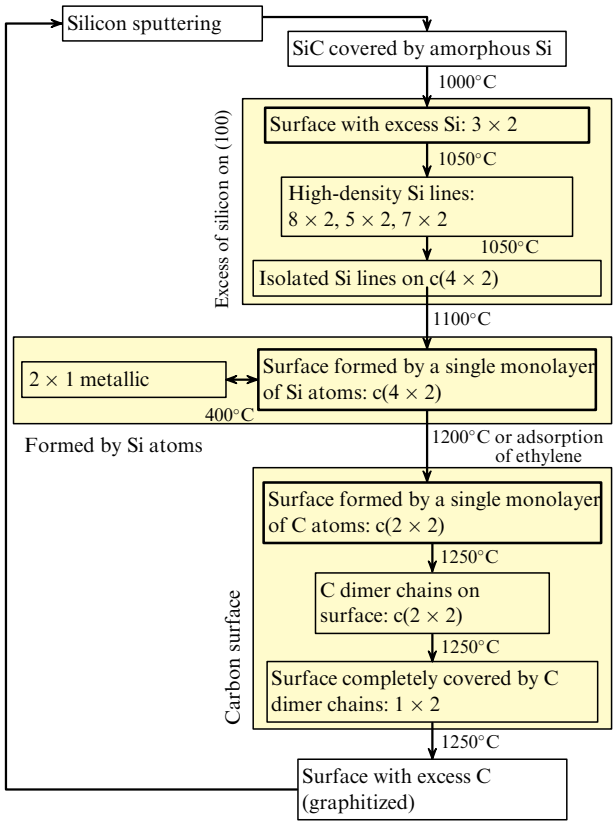

Figure A1. Sequence of fabricating superstructures on β-SiC(100) surface (according to Ref. [41]).

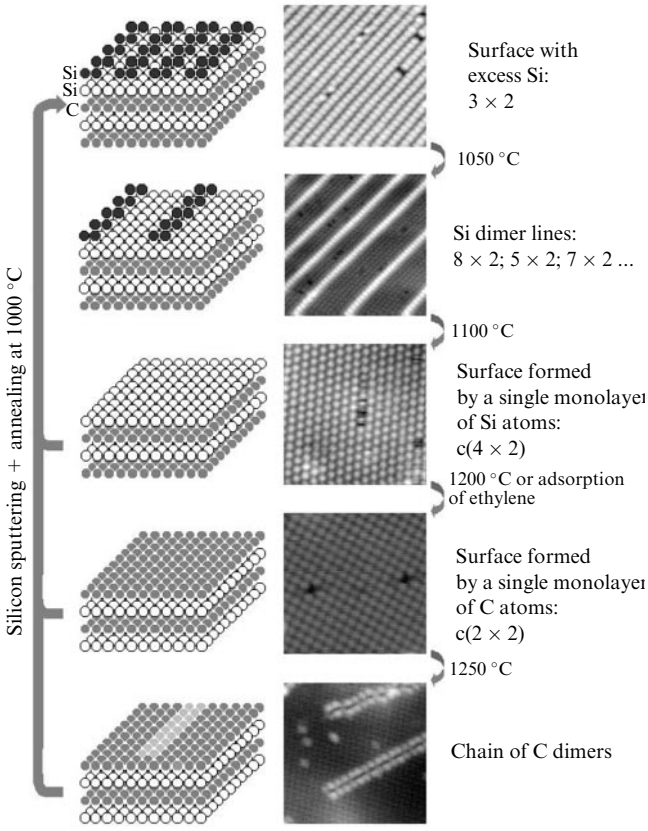

Figure A2. Superstructures on β-SiC(100) surface (according to Ref. [41]).

5. Proceedings of the 2nd European Conference on Silicon Carbide and Related Materials *Mat. Sci. Eng. B* **61–62** (1999); Proceedings of the International Conference on Silicon Carbide and Related Materials *Mat. Sci. Forum* **338–342** (1999); Proceedings of the 3nd European Conference on Silicon Carbide and Related Materials (in press)
6. Nanotechnology Research Direction, Vision for Nanotechnology R&D in the Next Decade, National Science and Technology Council. Interagency Working Group on Nanoscience, Engineering and Technology, Workshop report (1999)
7. *Nanotechnology* (Ed. G Timp) (New York: AIP Press, Springer, 1999)
8. Stroscio J A, Eigler D M *Science* **254** 319 (1991)
9. Dyan M *J. Vac. Sci. Technol. A* **3** 361 (1985); *A* **4** 38 (1986)
10. Bellina J J, Ferrante J, Zeller M V *J. Vac. Sci. Technol. A* **4** 1692 (1986)
11. Kaplan R, Parrill T M *Surf. Sci.* **165** L45 (1986)
12. Hara S et al. *Surf. Sci.* **231** L196 (1990)
13. Powers J M et al. *Surf. Sci.* **260** L7 (1992)
14. Wenchang L, Weidong Y, Kaiming Z *J. Phys.: Condens. Mat.* **3** 9079 (1991)
15. Carter S J N *Solid State Commun.* **72** 671 (1989)
16. Craig B I, Smith P V *Surf. Sci.* **233** 255 (1990)
17. Mehandru S P, Anderson A B *Phys. Rev. B* **42** 9040 (1990)
18. Badziag P *Phys. Rev. B* **44** 11143 (1991)
19. Yan H, Hu X, Jonsson H *Surf. Sci.* **316** 181 (1994)
20. Hu X et at. *J. Phys.: Condens. Mat.* **7** 1069 (1995)
21. Halicioglu T *Phys. Rev. B* **51** 7217 (1995)
22. Gutierrez R et al. *Phys. Rev. B* **60** 1771 (1999)
23. Sabisch M et al. *Phys. Rev. B* **53** 13121 (1996)
24. Käckell P, Furthmüller J, Bechstedt F *Surf. Sci.* **352–354** 55 (1996)
25. Catellani A, Galli G, Gygi F *Phys. Rev. Lett.* **77** 5090 (1996)
26. Kaplan R *Surf. Sci.* **215** 111 (1989); *J. Vac. Sci. Technol. A* **6** 829 (1988)
27. Shek M L *Surf. Sci.* **349** 317 (1996)
28. Semond F, Thése de Doctorat (Orsay: Universite de Paris-XI, 1996)
29. Soukiassian P et al. *Phys. Rev. Lett.* **78** 907 (1997)
30. Douillard L, Semond F, Aristov V Yu et al. *Mat. Sci. Forum* **264–268** 379 (1998)
31. Catellani A et al. *Phys. Rev. B* **57** 12255 (1998)
32. Lu W, Krüger P, Pollmann J *Phys. Rev. Lett.* **81** 2292 (1998)
33. Yoshinobu T et al. *Appl. Phys. Lett.* **59** 2844 (1991)
34. Soukiassian P, Aristov V Yu, Douillard L et al. *Phys. Rev. Lett.* **82** 3721 (1999): Comment: Lu W, Krüger P, Pollmann J *Phys. Rev. Lett.* **82** 3722 (1999) (Reply)
35. Aristov V Yu et al. *Phys. Rev. B* **60** 16553 (1999)
36. Joyce J J, Del Giudice M, Weaver J H *J. Electron Spectrosc. Related Phenomena* **49** 31 (1989)
37. Landemark E et al. *Phys. Rev. Lett.* **69** 1588 (1992)
38. Yeom H W et al. *Phys. Rev. B* **56** R15525 (1997); *Surf. Sci.* **433** 392 (1999)
39. Johansson L I, Owman F, Martensson P *Phys. Rev. B* **53** 13793 (1996)
40. Tromp R M, Smeenk R G, Saris F W *Surf. Sci.* **133** 137 (1983)
41. Derycke V, Thése de Doctorat (Orsay: Universite de Paris-XI, 2000)
42. Aristov V Yu et al. *Phys. Rev. Lett.* **79** 3700 (1997)
43. Aristov V Yu et al. *Omicron Newsletter* **1** 4 (1997)
44. Lu W, Krüger P, Pollmann J *Phys. Rev. B* **61** 2680 (2000)
45. Catellani A, Galli G, Gygi F *Appl. Phys. Lett.* **72** 1902 (1998)
46. Bermudez V M *Phys. Status Solidi B* **202** 447 (1997)
47. Kaplan R, Bermudez V, in *Properties of Silicon Carbide* (EMIS Datareview Series, Vol. 13, Ed. G Harris) (1995) p. 101
48. Soukiassian P, Semond F *J. Phys. IV* (*Colloque*) (France) **7** (C6) 101 (1997)
49. Pollmann J, Krüger P, Sabisch M *Phys. Status Solidi B* **202** 421 (1997)
50. Iijima S *Nature* **354** 56 (1991)
51. *Surface Science Techniques* (Eds J M Walls, R Smith) (Oxford: Pergamon Press, 1994)
52. Douilard L, Fauchoux O, Aristov V, Soukiassian P *Appl. Surf. Sci.* **166** 220 (2000)
53. Enriquez H, Derycke V, Aristov V Yu et al. *Appl. Surf. Sci.* **162–163** 559 (2000)
54. Haldane F D M *J. Phys. C* **14** 2585 (1981)
55. Voit J *Phys. Rev. B* **47** 6740 (1993)
56. *Electron Spectroscopies Applied to Low-Dimensional Structures* (Eds H I Starnberg, H P Hughes) (Dordrecht: Kluwer Acad. Publ., 2000)
57. Dardel B et al. *Europhys. Lett.* **24** 687 (1983)
58. Dardel B et al. *Phys. Rev. Lett.* **67** 3144 (1991)
59. Nakamura M et al. *Phys. Rev. B* **49** 16191 (1994)
60. Yan H, Smith A P, Jonsson H *Surf. Sci.* **330** 265 (1995)
61. Hara S et al. *Surf. Sci.* **357–358** 436 (1996)
62. Semond F et al. *Phys. Rev. Lett.* **77** 2013 (1996)
63. Lu W, Krüger P, Pollmann J *Phys. Rev. B* **60** 2495 (1999)
64. Lübbe M et al. *J. Vac. Sci. Technol. A* **16** 3471 (1998)
65. Yeom H W et al. *Phys. Rev. B* **58** 10540 (1998)
66. Yeom H W et al. *Phys. Rev. B* **61** R2417 (2000)
67. Pizzagalli L et al. *Phys. Rev. B* **60** R5129 (1999)
68. Shevlin S A, Fisher A J *Appl. Surf. Sci.* **162** 94 (2000)
69. Kitabatake M, Greene I E *Appl. Phys. Lett.* **69** 2048 (1996); *Jpn. J. Appl. Phys. Pt. 1* **35** 5261 (1996)
70. Douillard L, Aristov V Yu, Semond F, Soukiassian P *Surf. Sci. Lett.* **401** L395 (1998)
71. Soukiassian P et al. *Phys. Rev. Lett.* **79** 2498 (1997)
72. Semond F, Aristov V Yu, Douillard L et al. *Mat. Sci. Forum* **264–268** 387 (1998)
73. Aristov V Yu, Douillard L, Soukiassian P *Surf. Sci. Lett.* **440** L825 (1999)
74. Bellina J J (Jr.), Zeller M V *Appl. Surf. Sci.* **25** 380 (1986)
75. Hara S et al. *Surf. Sci.* **273** 437 (1992); *Thin Solid Films* **225** 240 (1993)
76. Fuyuki T, Yoshinobu T, Matsunami H *Thin Solid Films* **225** 225 (1993)
77. Hasegawa S et al. *Surf. Sci.* **206** L851 (1988)
78. Bermudez V M, Kaplan R *Phys. Rev. B* **44** 11149 (1991)
79. Powers J M et al. *Phys. Rev. B* **44** 11159 (1991)
80. Long J P, Bermudez V M, Ramaker D E *Phys. Rev. Lett.* **76** 991 (1996)
81. Yeom H W et al. *Phys. Rev. Lett.* **83** 1640 (1999); Shimomura M et al. *Surf. Sci.* **438** 237 (1999)
82. Craig B I, Smith P V *Surf. Sci.* **276** 174 (1992); Erratum, ibid. **285** 295 (1993)
83. Badziag P *Surf. Sci.* **269/270** 1152 (1992); *Diamond Relat. Mater.* **1** 285 (1992)
84. Halicioglu T *Thin Solid Films* **286** 184 (1996)
85. Dyson A J, Smith P V *Surf. Sci.* **396** 24 (1998)
86. Craig B I, Smith P V *Surf. Sci.* **256** L609 (1991)
87. Pollmann J et al. *Mater. Sci. Forum* **338–342** 369 (2000)
88. Pollmann J et al. *Appl. Surf. Sci.* **104–105** 1 (1996)
89. Käckell P, Furthmüller J, Bechstedt F *Appl. Surf. Sci.* **104–105** 45 (1996)
90. Käckell P et al. *Phys. Rev. B* **54** 10304 (1996)
91. Gutierrez R, Frauenheim Th *Mat. Res. Soc. Symp.* **423** 427 (1996)
92. Derycke V, Soukiassian P, Mayne A, Dujardin G *Surf. Sci. Lett.* **446** L101 (2000)
93. Derycke V et al. *Phys. Rev. Lett.* **81** 5868 (1998)
94. Catellani A, Galli G, Rigolli P L *Phys. Rev. B* **62** R4794 (2000)